PREPARATION AND CHARACTERIZATION OF MANGANITES

DISSERTATION

SUBMITTED IN PARTIAL FULFILLMENT OF THE REQUIREMENTS
FOR THE AWARD OF THE DEGREE OF

Master of Philosophy

IN

APPLIED PHYSICS

Submitted by

HILAL AHMED

Under the Supervision of

DR. SHAKEEL KHAN

DEPARTMENT OF APPLIED PHYSICS
FACULTY OF ENGINEERING & TECHNOLOGY
ALIGARH MUSLIM UNIVERSITY
ALIGARH (INDIA)

2008

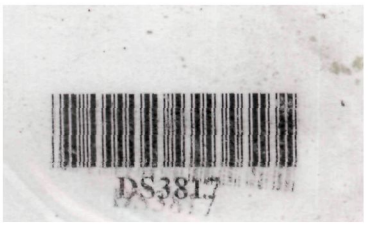


Dedicated
To
My Parents

DEPARTMENT OF APPLIED PHYSICS
Z. H. COLLEGE OF ENGG. & TECH.
ALIGARH MUSLIM UNIVERSITY
ALIGARH-202002

Date...05-11-2008

CERTIFICATE

Certified that the dissertation entitled, "Preparation and Characterization of Manganites" submitted by Mr. Hilal Ahmed is a record of the candidates own work carried out by him under my supervision and guidance. The results presented in this dissertation have not been submitted elsewhere and are suitable for the submission to the award of M. Phil. Degree.

Dr. Shakeel Khan

(Supervisor)

Department of Applied Physics

A.M.U., Aligarh

ACKNOWLEDGEMENTS

I feel privileged to produce my dissertation which would have not been possible without the grace of 'Almighty Allah' and the invaluable guidance and zealous efforts of my supervisor Dr. Shakeel Khan, Reader, Department of Applied Physics, Zakir Husain College of Engineering and Technology, Aligarh Muslim University, Aligarh.

I also feel obliged to Professor Alimuddin, Chairman, Department of Applied Physics, Zakir Husain College of Engineering and Technology, Aligarh Muslim University, Aligarh, for providing me all the required research facilities. I put on my record of thanks to all the teachers of department particularly to Dr. J. P. Srivastava (Emeritus Scientist, CSIR) who have always rendered their utmost help.

I would also like to express my heartfelt gratitude to the members of my family for their patience, inspiration and regular support throughout this work.

I am also grateful to my friends, Azizurrahman Ansari (I.I.T. Kanpur), Mohammad Shariq (I.I.T. Roorkee), Mohd. Asim Siddiqui, Prabal Pratap Singh Bhadhauria, Mohd. Jane Alam, Faheem Ahmad, Zameer Ahmed, Ritu Sharma, Nishat Arshi, Manisha Gupta, Haider Hasan Jafri (J.N.U.), Rajmani Gaur (I.I.T. Delhi), M. Firoz Khan, Sartaj Alam Ansari and Furqan Ahmad for putting forward their helping hands always.

At last but not least I would like to pay my heartiest thanks to Dr. M. Wasi Khan and Khan Zaheer (J.N.U.), for their kind help and creative suggestions.

Hilal Ahmed

CONTENTS

CHAPTER-IV CONCLUSIONS

CHAPTER-1

INTRODUCTION

1.1 INTRODUCTION AND HISTORICAL BACKGROUND:

During the last decade, interest has grown in heterogeneous ferromagnetic materials, such as thin film multilayers and cluster alloy compounds which display the so called giant magnetoresistance (GMR). More recently, it has been recognised that some materials specifically 3d transition metal oxides, posses large room temperature magnetoresistivity associated with a paramagnetic-ferromagnetic phase transition. The compounds which have been the focus of the majority of the studies are the magnetic perovskites $R_{1-x}A_xMnO_3$ where R is a trivalent rare earth cation (e.g.-La, Pr, Sm, Nd, etc) and A is a divalent alkaline earth cation (e.g.-Ca, Sr, Ba, Pb etc).

Since after the discovery of superconductivity in lanthanum cuperates, the perovskites materials have received much attention. The existence of metal-insulator transition (MIT) in lanthanum based manganites was established in early 1950's [1, 2], and was extensively studied thereafter. Transition metal perovskites present a very interesting group of materials because of extremely rich variety of their electrical properties, from a large gap insulator to metal and magnetic properties such as non magnetism to magnetism, antiferromagnetism to ferromagnetism. [3, 4]. These phenomena have been observed in a family of doped manganites.

1.1.1 PEROVSKITES:

Perovskites form the most important class of ferroelectric materials. Manganites crystallize in a 'perovskite' structure. They are named after the mineral perovskite $CaTiO_3$ (it was discovered later that $CaTiO_3$ shows only a distorted perovskite structure). The perfect structure follows the formula ABO_3, where A is a mono or divalent and B is a tetra or pentavalent metal. As shown in Fig 1.1, the A atoms form the corners of the cubic cells and B atoms are in the centre and the oxygen atoms are situated in the centres of faces. As the B atoms are

enclosed in O_6 octahedra, this structure is also regarded as BO_6. Many superconducting ceramic materials especially cuperate superconductors also have perovskite type structures.

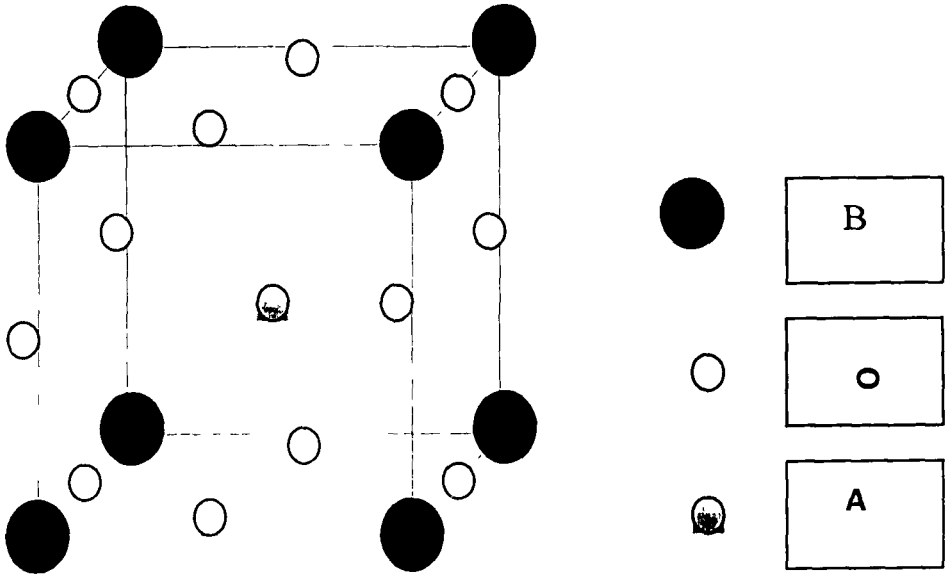

Fig 1.1: The structure of a typical ABO_3 type compound

The stability of a perovskite structure depends on the tolerance factor defined by:

$$t = (r_A+r_O)/\sqrt{2}(r_B+r_O) \qquad (1.1)$$

Where r_A, r_B & r_O being the radii of A, B cations and oxygen ions respectively. Perovskite structure is supposed to be stabilized in the range of $0.75 < t \leq 1.0$. However, for an ideal perovskite $t = 1$. For $t < 1$, the cubic structure transforms to the orthorhombic structure which leads to deviation in Mn-O-Mn bond angle from 180^0 (a case for ideal perovskite). As tolerance factor decreases, the tendency to charge localization increases due to reduction in carrier mobility. The manganites of the type $R_{1-x}A_xMnO_3$ have attracted the attention of the

scientific community due the "colossal magnetoresistance" (CMR) phenomenon exhibited when the ferromagnetic ordering of Mn spins occurs [5, 6].

1.1.2 MAGNETORESISTANCE (MR), GIANT MAGNETORESISTANCE (GMR) AND COLOSSAL MAGNETORESISTANCE (CMR):

Magnetoresistance (MR) is the relative change in the electrical resistivity of a material produced by the application of a magnetic field. It is generally defined as:

$$\mathbf{MR} = \Delta\rho/\rho(0)=\{\rho(H)-\rho(0)\}/\rho(0) \qquad (1.2)$$

where $\rho(H)$ and $\rho(0)$ are the resistivities at a given temperature in the presence and absence of a magnetic field respectively. MR can be negative or positive. Most metals show a small MR (only a few %). In non-magnetic pure metals and alloys, MR is general'y positive and it shows a quadratic dependence on H. MR can be negative in magnetic materials because of the suppression of the spin disorder by the magnetic field.

Large magnetoresistance, referred to as Giant magnetoresistance (GMR) was first observed on the application of magnetic field to atomically engineered magnetic super lattices (e.g.-Fe/Cr) [7] and in magnetic semiconductors. Besides some of the bimetallic or multi-metallic layers, comprising of ferromagnetic and antiferromagnetic or nonmagnetic metals, GMR is also found in ferromagnetic granules dispersed in paramagnetic metal films. The discovery of negative GMR in rare-earth manganites $R_{1-x}A_xMnO_3$ with the perovskite structure has attracted wide attention.

GMR has found applications for these materials in device applications such as (i) magnetic recording (memory storage), (ii) actuators and (iii) sensors. The first observation concerning GMR was made in respect of Fe/Cr multilayers [8] with thin Cr layers; prepared by molecular beam epitaxy (MBE).

For Cr layers of 9 angstroms thickness, the resistivity was found to drop by almost a factor of 2 in a magnetic field of 2 Tesla at 4.2 K as shown in Fig. 1.2, giving a negative GMR of about 50 percent. Another term 'Colossal Magnetoresistance' (CMR) is often used to describe the extremely strong influence of the magnetic field. The CMR is defined as

$$\Delta\rho/\rho\,(H) = \{\rho\,(H)-\rho\,(0)\}/\rho\,(H) \qquad (1.3)$$

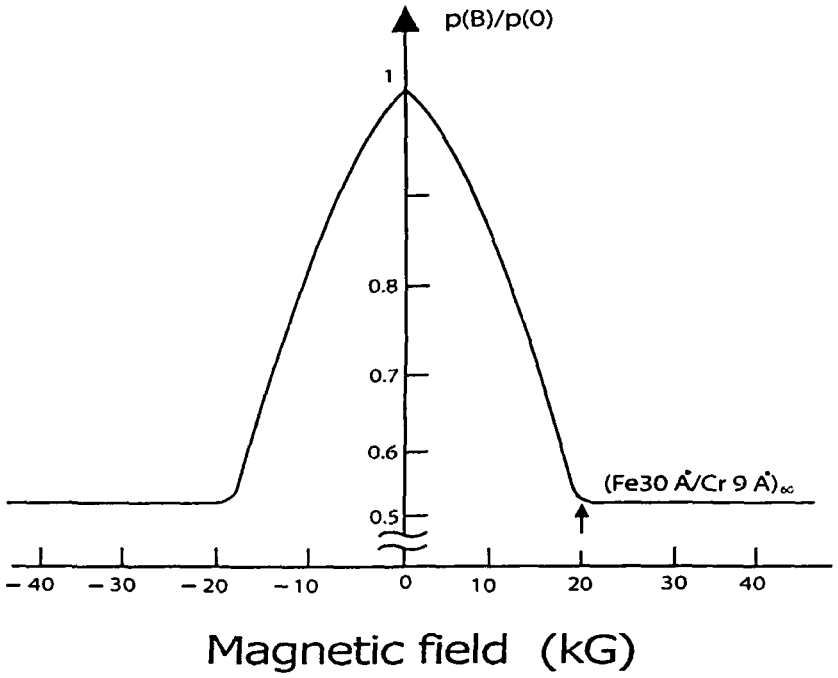

Fig. 1.2 Variation of resistivity of multilayers [(001) Fe 30 angstroms/ (001) Cr 9 angstroms]$_{60}$ as a function of the magnetic field at 4.2K. The specimen is a super lattice of 60 bilayers in which the current flows along the (110) direction and the magnetic field is applied in the layer plane (001) along the current direction. At the magnetic field B_s (in the saturated state; B_s = 2T) the resistivity drops to almost half its zero field value.

The CMR reaches its maximum (in access of 10^6 percent) at 110 K with the magnetic field at 6 Tesla as shown in Fig. 1.3. The peak occurs just below the Curie temperature. For films thicker than 2000 angstroms, the MR is

reduced by orders of magnitude. The presence of grain boundaries leading to lattice strain is detrimental to achieve large MR. The MR improves further on heat treatment.

The two most striking features of the GMR-CMR effects in manganites are as under;

(i) Firstly, the MR peak can be shifted to occur at room temperature by adjusting the processing parameters.

(ii) Secondly, the resistivity can be manipulated by magnetic field to change by orders of magnitude.

The magnetic and transport properties of these samples are determined by several factors such as the percentage of the divalent ions, the ionic radii of the metal ions and the method used in the preparation of samples etc [10, 11]. These properties have traditionally been examined within the framework of the "Double-Exchange" (DE) mechanism proposed by Zener[12] which considers the magnetic coupling between Mn^{+3} and Mn^{+4} changing due to doping level in the perovskite or its oxygen stoichiometry. In both cases the result is a distortion of the pervoskite structure that has direct influence not only on the Mn-O distance but also on the angle of the Mn^{+3}-O-Mn^{+4} bond. It has also been observed that the ferromagnetic coupling and the metal-insulator transition temperature are very sensitive to the change of these parameters. Although some researchers [13, 14] believe that the DE model is very rough and could not explain alone very large resistivity of the insulating phase for $T>T_c$, it still remains the main and essential theoretical mechanism used to explain the anomalous phenomena. There are a lot of possibilities of technological applications of these materials due to their interesting properties mentioned above. In view of this fact many new experiments are being performed and new

materials with similar properties searched for a precise understanding of the origin and mechanism of these effects.

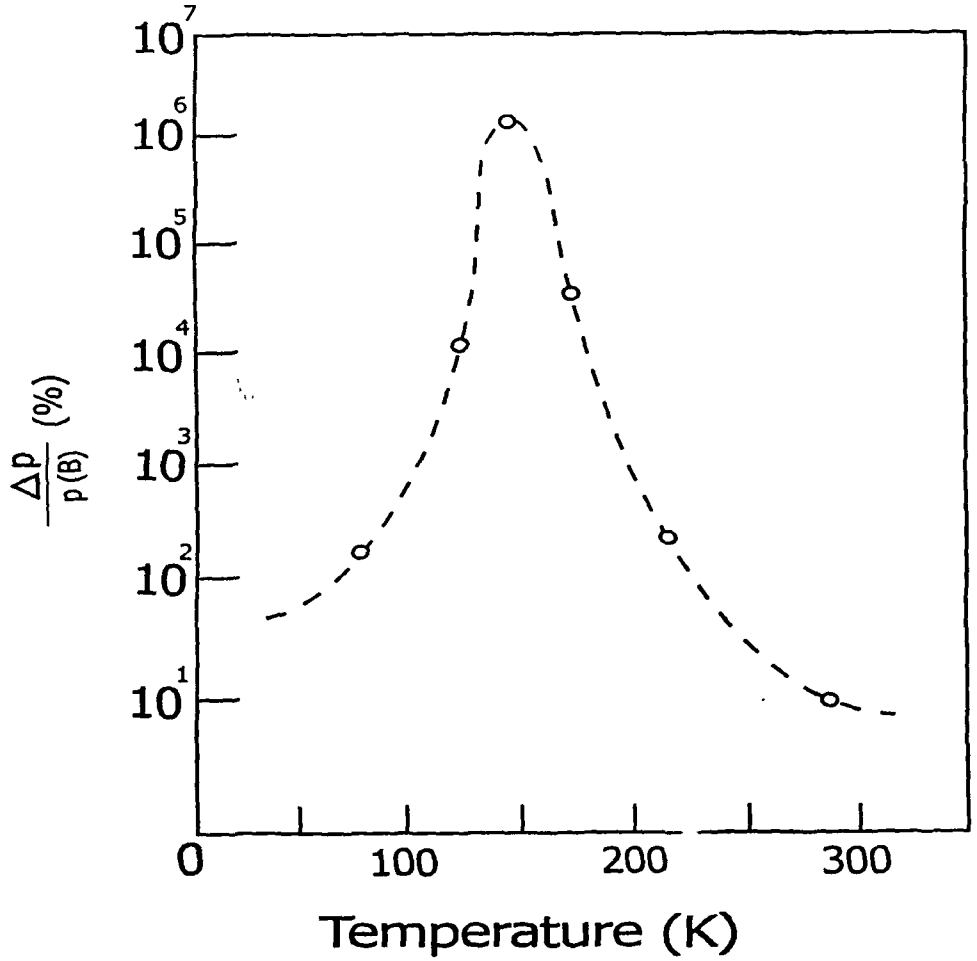

Fig .1.3 *Variation of magnetoresistance of a thin film of La-Ca-Mn-O as a function of temperature. The MR peaks at 110K in a magnetic field of 6T. [After S. Jin, et al.[9], Appl. Phys. Lett., 67, 557, (1995)]*

1.2 THEORETICAL MODELS:

The basis for the theoretical understanding of Mn oxides is usually the concept of the double exchange (DE) [12] that considers the exchange of electron between neighbouring Mn^{3+} and Mn^{4+} sites with strong on-site Hund's coupling. Attempts based on mean field treatments of a Kondo lattice model for DE [15] and a Hubbard-Kondo lattice model [16] have been made to account for the

transport properties of Mn oxides. However, the sharp change in the resistivity and the CMR near T_C were not reproduced successfully in these reports. Perturbative calculations carried out by Millis et al [13, 17] showed that DE alone could not explain the experimental data of Mn oxides and suggested that a strong Jahn-Teller distortion should be responsible for the transport properties. Later on it was suggested that the localization effect [18, 19] in the double exchange model based upon non-perturbative treatments might be able to account for the novel properties of manganites.

1.2.1 DOUBLE EXCHANGE INTERACTION:

The magnetic and electronic properties have traditionally been examined within the framework of the double exchange model that considers the magnetic coupling between Mn^{3+} and Mn^{4+} resulting from the motion of an electron between the two partially filled d shells with strong on-site Hund's coupling.

All unpaired electrons within each atom or ion strive to attain the configuration of a lowered energy state in which, according to Hund's rule, all spins are parallel to one another. Since the conduction electrons carry along their own spins unchanged as they move from atom to atom, they are able to move within an environment of parallel spins only if the spins of all the incomplete d-shells point in the same direction. This indirect coupling via the conduction electrons will therefore lower the energy of the system when the spins of the d-shells are all parallel. This model also assumed that the direct coupling between incomplete d-shells always tends to align their spins antiparallel. It was thereby predicted that ferromagnetism would never occur in the absence of conduction electrons.

The pure $LaMnO_3$ shows the semiconducting property. When some of the La^{3+} ions are replaced by divalent ions like Ca^{2+} ions, it is necessary that a

corresponding number of Mn^{3+} ions be replaced by Mn^{4+} ions to preserve the charge neutrality.

Then, if we define Ψ_1 and Ψ_2 as follows

Ψ_1: $Mn^{3+}\, O^{2-}\, Mn^{4+}$

Ψ_2: $Mn^{4+}\, O^{2-}\, Mn^{3+}$

Since $\Psi_1$and Ψ_2 are degenerate functions, more exact waveforms will be obtained by taking the linear combinations.

$$\Psi_+ = \Psi_1+\Psi_2 \qquad ; \qquad \Psi_- = \Psi_1-\Psi_2 \tag{1.4}$$

The energy difference of these two linear combinations is represented by 2ε; ε being the exchange energy, given explicitly b

$$\varepsilon = \int \Psi_1^{*}(H - \varepsilon_0)\, \Psi_2\, d\tau \tag{1.5}$$

where H is the Hamiltonian of the whole system and ε_0 is the energy associated with the initial states $\Psi_1$and Ψ_2. The above integral known commonly as the exchange integral extends over the coordinates and the spins of all the electrons. The integral (1.5) is non vanishing only if spins of the two d-shells are parallel. The lowest energy of the system thus corresponds to a parallel alignment of electron spins in Mn^{3+} and Mn^{4+}. It can be concluded that the lining up of the spins adjacent to incomplete d-shells of the Mn ions will be accompanied by an increase in the rate of migration of Mn^{4+} ions and hence by an increase in the electrical conductivity. Further, it should be realized that a stationary state is represented neither by $\Psi_1$nor by Ψ_2 but by either of the two linear combinations as shown in (1.4).

Depending upon the sign of the exchange integral (1.5), the double exchange raises the energy associated with Ψ_+ and lowers the energy associated with Ψ_- or vice-versa. Thus the energy of one of these two stationary states is lowered by the double exchange, which takes place when the d-shell spins are parallel. However, at low temperatures, regardless of the sign of the exchange integral, the energy of the system will be lowered by a parallel alignment of spins. The rate at which electron jumps from a Mn^{3+} ion across an intervening O^{2-} ion to an adjacent Mn^{4+} ion is given by the frequency;

$$\nu = 2\,\varepsilon/h$$

The diffusion coefficient for the Mn^{4+} ion is thus given by

$$D = a^2\varepsilon/h \qquad (1.6)$$

where 'a' is the lattice parameter. From Einstein relation

$$\sigma = ne^2\,D/kT$$

where σ = electrical conductivity

D = diffusion coefficient

n = no. of ions (Mn^{4+}) per unit volume

Electrical conductivity can be written as

$$\sigma = xe^2\,\varepsilon\,/ahkT \qquad (1.7)$$

Here x is that fraction of Mn ions which have 4+ charges.

The Curie temperature T_C is approximately given as

$$kT_C \approx \varepsilon \qquad (1.8)$$

From (1.7) and (1.8)

$$\sigma = (xe^2/ah)\,(T_C/T)$$

This relation correlates the conductivity (σ) and Curie temperature (T_C) for manganites.

1.2.2 JAHN-TELLER EFFECT:

Jahn-Teller theorem [20] states that, "For a nonlinear molecule in an electronically degenerate state, distortion must occur to lower the symmetry, remove the degeneracy and lower the energy.

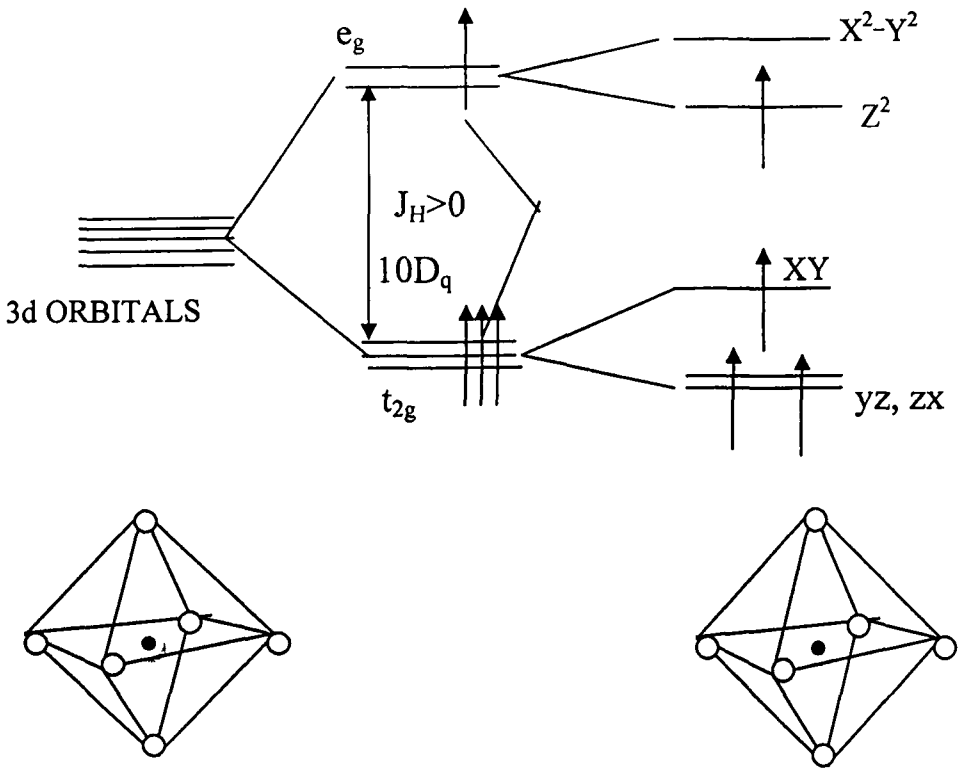

Fig.1.4 Field splitting of the five-fold degenerate atomic 3d levels into lower t_{2g} and higher e_g levels. The particular Jahn-Teller distortion sketched in the figure further lifts each degeneracy as shown.

In the Jahn-Teller effect, a distortion of the oxygen octahedron surrounding the B- site cation splits the energy levels of a 3d ion such as Mn, thus lowering the energy. The distorted structures are frequently orthorhombic.

Divalent cations which can occupy the body-centered A-site including calcium, barium, strontium and lead; trivalent cations include yttrium, lanthanum, praseodymium, neodymium and some other rare-earths (La).

Besides manganese, many perovskite structures form with aluminium, gallium or another 3d element such as-chromium, iron, cobalt or nickel on the B sites. The rare-earth orthoferrits $LaFeO_3$ are one example of a series of perovskite structure oxides. There are many others. Any of the trivalent 3d cations can be substituted partially for manganese.

The Jahn-Teller polaron can form in a solid when the Jahn-Teller stabilization energy δ_{JT} is comparable with the conduction electron bandwidth W. Unlike the dielectric polaron where a charge polarization decorates the carriers and a local isotropic distortion increases their effective mass, the Jahn-Teller polaron carries with it, an anisotropic local distortion which removes the degeneracy of the electronic ground state.

In manganese oxides where apical O-atoms move towards the Mn-ion, the energy of d_z^2 becomes higher than that of d_x^2-$_y^2$ and the degeneracy is lifted as shown in Fig 1.4. This is called Jahn-Teller effect and is represented by the following Hamiltonian for a single octahedron.

$$H_{JT} = -g\,(T_X Q_2 + T_Z Q_3) \qquad (1.9)$$

where (Q_2, Q3) are the coordinates for the displacement of O-atoms surrounding the transition metal atoms and g is the coupling constant. T_X,T_Z are the x and z component of orbital pseudo spins. When a crystal is considered, (Q_2, Q3) should be generalized to (Q_{i2},Q_{i3}) (where 'i' is site index) which is represented as the sum of the phonon coordinates and the uniform component (u_2,u_3). Here (u_2,u_3) describes the crystal distortion as a whole. In $La_{1-x}A_xMnO_3$ the electrically active orbitals are the Mn d_x^2-$_y^2$ and d_z^2 orbitals (as shown in Fig. 1.4). The Hund's rule coupling is believed to be very strong relative to the

d-d hopping and the spin orbit coupling. So, the spins of all of the d-electrons on a given site must be parallel. Three of the d-electrons go into the tightly bound core (d_{xy}, d_{xz}, d_{yz} orbitals , Fig. 1.4 forming a core spin S_i^3 of magnitude 3/2), to which the outer shell electron which may hop from site to site) is aligned by the Hund's rule coupling. The Hamiltonian containing this Physics is-

$$H_{d\text{-}ex} = \sum t^{ab}_{ij} d^{+}_{ia\acute{\alpha}} d_{jb\acute{\alpha}} - J_H \sum Si^{C} d^{+}_{ia\acute{\alpha}} \zeta_{\acute{\alpha}\beta} d_{i\acute{\alpha}\beta} \qquad (1.10)$$

Here $d^{+}_{ia\acute{\alpha}}$ creates an electron in an outer shell orbital state a, b=x^2-y^2 or z^2 and spin $\acute{\alpha}$, J_H is the Hund's rule coupling connecting the core spin to the outer shell electrons. t^{ab}_{ij} is the transfer integral which depends on the direction of the bond ij and also on the pair of the two orbitals a, b=(x^2-y^2) or z^2.

1.2.3 ELECTRONIC LOCALIZATION EFFECT:

The manganites are modelled as systems with both DE off diagonal disorder and non-magnetic diagonal disorder [18, 19] with the help of scaling theory and assuming a mean field distribution for the spin orientation, the localization length of electron can be evaluated as a function of magnetization. The resistivity in the variable range hopping (VRH) regime is calculated as a function of temperature for different values of applied magnetic field. In the manganites, two features apart from the known spin disorder might be important for the electronic localization. The substitution of R^{3+} with Ca, Ba, and Sr may lead to a local potential fluctuation. A rough estimate [21] shows that this potential fluctuation may be comparable with the width of the e_g band. The other feature is the lattice distortion around A^{2+} and R^{3+} due to their different

ionic sizes. These two effects give rise to a rather strong nonmagnetic electron-impurity scattering potential. Based on the above mentioned considerations a Hamiltonian was proposed to describe the transport behaviour of the e_g electrons in manganites.

$$H_{eg} = -\sum_{ij} t_{ij}\, d_i^{+} d_j + \sum_i \varepsilon_i d_i^{+} d_i \qquad (1.11)$$

Here the first term is the effective DE Hamiltonian in which

$$t_{ij}=t\{\cos(\theta_i/2)\cos(\theta_j/2)+\sin(\theta_i/2)\sin(\theta_j/2)\exp[i(\Phi_i-\Phi_j)]\} \qquad (1.12)$$

where 't' is the hopping integral in the absence of Hund's coupling and the polar angles (Φ_i, Φ_j) characterize the orientation of the local spin S_i .

1.2.4 TOLERANCE FACTOR:

The "tolerance factor" being a geometrical factor, plays an important role in manganites and related materials. There are two characteristic distortions that influence the perovskite structure (ABO_3) of manganites. One of these distortions results from the cooperative tilting of MnO_6 octahedra. This distortion is a consequence of the mismatch of the ionic radii. The Goldschmidt tolerance factor,'t' is defined as [22].

$$t = (r_A+r_O)/\sqrt{2}\,(r_B+r_O)$$

where r_A, r_O and r_B represent the ionic radii of rare-earth ion, oxygen and Mn respectively. It is a measure of distortion from the cubic symmetry.

The tolerance factors for some of the manganites are given in table below;

S.No.	Compound	Tolerance factor (t)
1.	$LaMnO_3$	0.889
2.	$PrMnO_3$	0.868
3.	$NdMnO_3$	0.864
4.	$SmMnO_3$	0.858

In the parent compound $LaMnO_3$, the Mn ions occupy the B site and are surrounded by oxygen octahedral that shares corners to form a three dimensional network. The La ion occupies the A site between these octahedral. In several perovskites, the overlap between the B site d orbital and the oxygen p orbital forms the electronically active band and this overlap can be strongly influenced by the internal pressure by the A-site substitution with ions of different radii. Mainly the effect of decreasing $<r_A>$ is to decrease the Mn-O-Mn bond angle reducing thereby the matrix element 'b' which describes the electron hopping between Mn sites. As discussed above, the tolerance factor is a

simple characterization of the size mismatch that occurs when the A ions are too small to fill the space in the three dimensional network of MnO_6 octahedra. For a perfect size match (t=1), the Mn-O-Mn bond angle (θ) would be 180^0. For $t< 1$, rather than giving a simple contraction of bond lengths, the octahedral tilts and relates to reduce the excess space around the A–site resulting in $\theta<180^0$. The apparent decrease in 'b' with decreasing $<r_A>$ originates from the decrease in θ. The band width W of e_g electrons, which affects the transition temperature (T_C) is controlled by both the Mn-O bond length and the bond angle θ of the Mn-O-Mn. The fine tuning of W and T_C can be obtained by appropriate selection of the size of rare-earth ion. This affects the bond angle θ and not the bond length due to the local disorder in the lattice. The application of external hydrostatic pressure compresses bond length and opens up θ, enhancing the bandwidth W.

1.2.5 PHASE DIAGRAMS:

The properties of the perovskite manganites such as $La_{1-x}Ca_xMnO_3$ and $La_{1-x}Sr_xMnO_3$ depend on the concentration of dopants x, and the temperature. Depending on the doping level (x) and the temperature, these systems present different phases of conduction and complicated magnetic phase transitions. The changes in the electronic and magnetic properties of the manganites with the change in composition have been worked out in several systems. On the basis of these measurements typical phase diagrams for Ca and Sr doped systems of

$LaMnO_3$ are shown in Fig. 1.6(a) and 1.6(b). The material is always paramagnetic above the transition temperature. The undoped compound (x=0) is insulating and a layered antiferromagnet. On the nominal doping with divalent alkaline elements like Ca, Sr, Ba (x<0.2) complex structures are observed and under certain conditions the material can be a metallic ferromagnet. As the amount of doping increased, the material becomes ferromagnetic below the Curie temperature. The ferromagnetic coupling is strongest at x = 0.3-0.4, the point at which the Curie temperature reaches its maximum value. At low doping (x<0.2) the material behaves like a semiconductor, showing an increase in resistivity as the temperature is lowered.

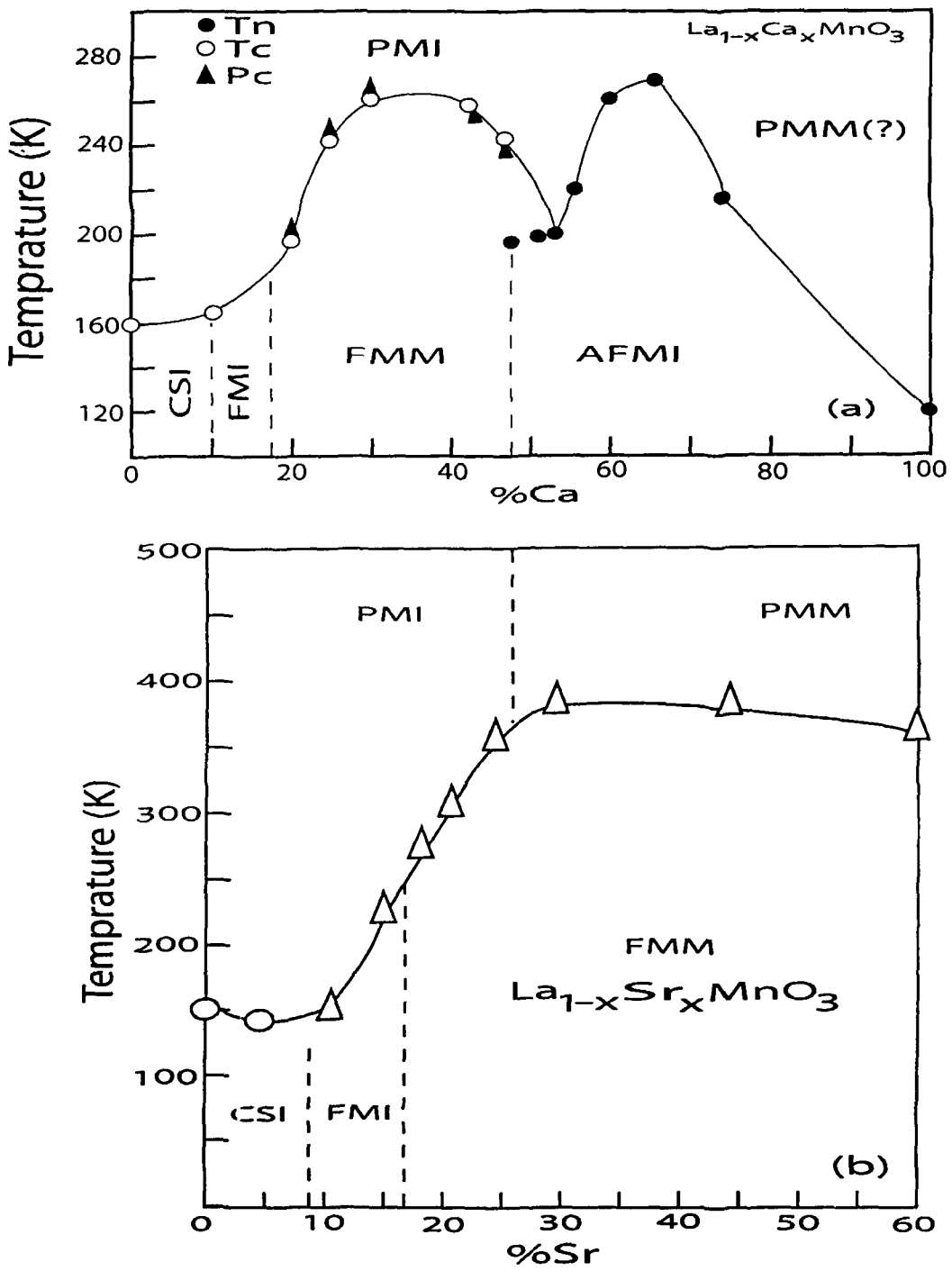

Fig.1.6 The phase diagrams of $La_{1-x}A_xMnO_3$ (A = Ca, Sr)

For increased doping, however, there is a tendency towards metallic conductivity, as observed for $La_{0.67}Sr_{0.33}MnO_3$ in the paramagnetic phase. In the high doping region (x>0.5) an insulating and antiferromagnetic charge ordered state is formed.

The transition from the paramagnetic to the ferromagnetic state is also accompanied by a sudden reduction in the resistivity. Such a drop is well known in other ferromagnetic metallic systems and is caused by the transition from a state with spin disorder to one with ordered spin. Disorder causes charge carriers with different spin orientations to scatter from each other, increasing the resistivity. The same loss of resistivity should be observed in an applied magnetic field; since this aligns the electrons spins and also prevents the scattering caused by spin disorder.

Since three of the electrons in the 3d orbital of the manganese ions form a triplet state at a lower energy. These electrons are treated as localized electrons that remain bound to the ion, and because their spin point in the same direction, they have an overall magnetic moment of 3/2. While the electrons in the highest energy level are shared with the oxygen ions, forming an energy band that extends through out the solid. The motion of charge carriers through this energy band and hence the conductivity of the material is largely controlled by the width of the band. This is determined by the overlapping of the manganese and oxygen orbitals, which in turn depends on the geometrical arrangement of the ions. A large overlap creates wide band. For a given distance between manganese and oxygen ions, the overlap is largest when the Mn-O-Mn bond angle is 180^0. Such an arrangement is found in an ideal perovskite structure in which manganese and six oxygen ions form a regular octahedron. But if the lanthanum is replaced with a smaller ion, the octahedron distorts and the bond angle becomes smaller. This decreases the overlap between the orbitals and narrows the energy band. Materials with narrow energy bands also show weaker ferromagnetic coupling, leading to a lower Curie temperature.

The alignment of electron spins modifies the effective bandwidth of manganites. It is easier for electrons to hop between Mn^{3+}/Mn^{4+} sites when the localized moments in neighbouring ions are aligned. Thus the effective

bandwidth and the conductivity increases when the material becomes magnetically ordered below the Curie temperature. The ferromagnetic coupling in these materials is therefore transmitted via mobile carriers. When charge carriers are not free to move, the system is insulating and the interaction between the localized electrons induce antiferromagnetic order below the *Ne'el* temperature.

Electrical, magnetic and other measurements on $La_{1-x}A_xMnO_3$ systems have revealed certain unusual features with respect to charge carriers in these oxides. For example, the manganites exhibit very high resistivity particularly at low temperatures (<100 K) [21]. The values of resistivity are considerably higher than Mott's maximum value of resistivity [23], the resistivity reaching a value of 10^3-10^4 ohm-cm in the so called metallic state.

The resistivity in the ferromagnetic regime of manganites has been investigated by a number of workers. Just below T_C, it varies rapidly with temperature. For $T < 0.5\ T_C$, the variation is less rapid and is different from what is generally seen in a metallic ferromagnet. In general, for $T < 0.2T_C$, T^2 dependence seems to make the major contribution.

REFERENCES

1. G. H. Jonker and J.H. van Santen; Physica **16** (1950) 337

2. J.H. van Santen and G.H. Jonker; Physica **16** (1950) 599

3. G. Pari, S.M. Jaya, G. Subramoniam and R. Asokamani, Phys. Rev. **B51** (1995) 16575

4. D.D. Sharma, N. Shanthi, S.R. Barman, N. Hamada, H. Sawadana, K. Terakura, Phys. Rev. Lett. **75** (1995) 1126

5. H.Y. Hwang, S.-W. Cheong, P.G. Radaelli, M. Marezio and B. Batlogg, Phy. Rev. Lett. **75** (1995) 914

6. P. Schiffer, A.P. Ramirez, W. Bao and S.-W. Cheong, Phy. Rev. Lett. **75** (1995) 3336

7. P. M. Levy; Solid State Physics, **47** (1994) 367

8. M.N. Baibich et al, Phy. Rev. Lett. **61** (1988) 2472

9. S. Jin et al. Appl. Phys. Lett. , **67** (1995) 557

10. Nestor E. Massa, Horacio Falcon, Horacio Salva, Raul E. Carbanio Phys. Rev. **B56** (1997) 10178

11. L. Righi, P. Gorria, M. Insausti, J. Gitirrez and J.M. Barandiaran, J. Appl. Phys. **81** (1997) 5767

12. C. Zener, Phys. Rev. **82** (1951) 403

13. A.J. Millis, B.I. Shrainman and R. Mueller, Phys Rev. Lett. **77** (1996) 175

14. L. Sheng, D.Y. Xing, D.N. Sheng and C.S. Ting Phys. Rev. Lett. **79** (1997) 1710

15. N. Furukawa; J. Phys. Soc. Japan, **63** (1994) 3214

16. J. Inove and S. Maekawa; Phys. Rev. Lett., **74** (1995) 3407

17. A.J. Millis, P.B. Littlewood and B.I. Shraiman; Phys. Rev. Lett. **74** (1995) 5144

18. E. Mueller-Hartmann and E. Doggoto; Phys. Rev. **B54** (1996) E6819

19. C.M. Varma; Phys. Rev. **B54** (1996) 7328

20. H.A. Jahu and E. Teller; Proc. Roy. Soc. **A161** (1937) 220

21. J.M.D. Coey, M. Viret, L. Ranno, K. Ounadjela; Phys. Rev. Lett. **75** (1995) 3910

22. N.R. Rao and B. Reveau; Colossal magnetoresistance, charge-ordering and related properties of manganese oxides; World Scientific Publications (1998)

23. R. Mahendiran, S.K. Tiwary, A.K. Raychaudhury, T.V. Ramakrishnan, R. Mahesh, N. Rangavittal, C.N.R. Rao; Phys. Rev. **B53** (1996) 3348

CHAPTER-2

EXPERIMENTAL TECHNIQUES

2.1 INTRODUCTION:

This chapter deals with the method of preparation and characterization of manganites samples $La_{1-x}Ca_xMnO_3$ (x=0.25, 0.33, 0.40, 0.45, 0.50, 0.55, 0.60), $La_{1-x}Ba_xMnO_3$(x=0.10, 0.15, 0.20, 0.33, 0.45) and also $La_{1-x}Sr_xMnO_3$(x=0.25, 0.33, 0.40, 0.50). For sample preparation, the conventional solid state reaction route [1, 4]. Sol-Gel method [5] (Wet chemical reaction method) and coprecipitation [6, 7] is also used to synthesize the perovskite manganites. Various techniques used to characterize these samples are described briefly viz: X-Ray Diffraction, Four-Probe for Resistivity measurements and Vibrating Sample Magnetometer (VSM) for magnetization measurements.

2.2 SYNTHESIS OF BULK SAMPLES:

Samples of manganites in our program were prepared by Solid-State reaction route as well as Sol-Gel method.

2.2.1 DESCRIPTION OF SOLID STATE REACTION ROUTE:

In the solid-state reaction route different constituents are mixed in stoichiometric ratio and heated at high temperatures to complete the reaction.We have prepared the samples of $La_{1-x}Ca_xMnO_3$ (x=0.25, 0.33, 0.40, 0.45, 0.50, 0.55, 0.60), $La_{1-x}Ba_xMnO_3$ (x=0.10, 0.15, 0.20, 0.33, 0.45) and $La_{1-x}Sr_xMnO_3$ (x=0.25, 0.33, 0.40, 0.50) by the solid-state reaction route which has been summarized in the form of flow chart as shown in Fig.2.1;

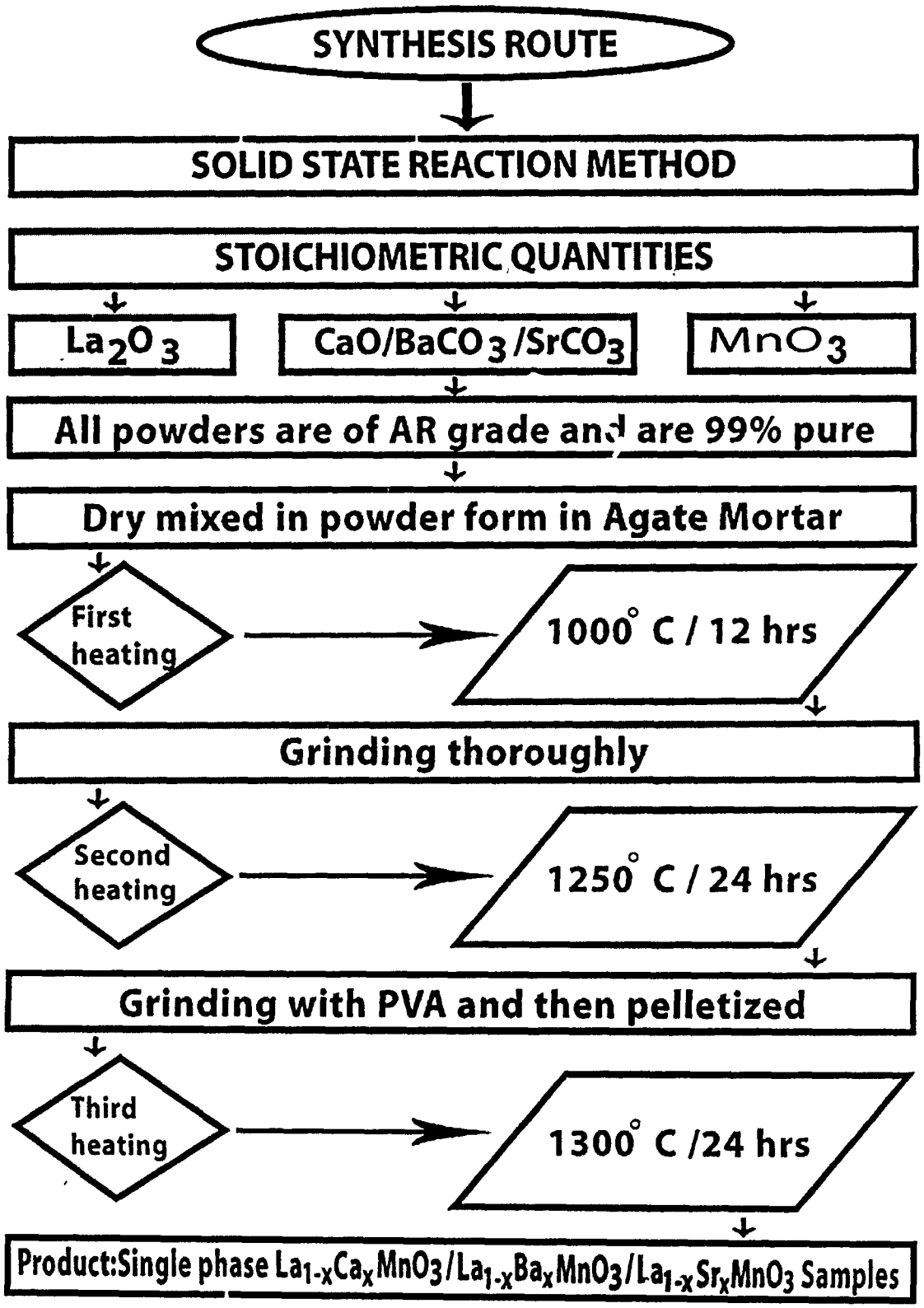

Fig. 2.1 Flow chart for Solid-state reaction route used for synthesis of bulk samples.

The stoichiometric amounts of La_2O_3, $CaO/BaCO_3/SrCO_3$ and MnO_3 (all of AR grade) in powdered form were ground in an agate mortar till a homogeneous mixture was formed. This mixture was kept in a crucible and heated at 1000^0C for about 12 hrs. The pre sintered material were again ground and calcinated at 1250^0C for 24 hrs. This preheated powder was tried for making pellets but pellets could not be formed so few drops of PVA (poly vinyl alcohol) which act as a binder in the sample were added in the powder and palletized using a rectangular die of dimensions 15mm×4mm×2mm at a pressure of the order of 3 tons/cm^2. Then, these pellets were sintered at 1300^0C for 24 hrs. The single peak nature of the samples was studied using the Powder X-Ray diffraction technique.

2.2.2 DESCRIPTION OF SOL-GEL METHOD:

To prepare samples by Sol-Gel method first different constituents were weighed in stoichiometric ratio and then preparation was done in following steps. We have prepared a series of $La_{1-x}Sr_xMnO_3$ (x = 0.25, 0.33, 0.40).

- To make dilute solution of Nitric Acid.
- To make a solution of Citric Acid in distilled water.
- The material was taken in a beaker and then nitric acid was added into it slowly and the mixture was heated at 77 ^0C till the solution became homogeneous i.e. material was completely dissolved in nitric acid (material should not rest at the bottom of the beaker).
- Now citric acid and ethylene glycol was added in 3:1 ratio to the above solution and heated it up to 227^0C till the solution became gelatinous.
- The gelatinous solution was heated till the material became dry.

- Dried material was heated further for 3 hrs up to 527^{0}C (800K) to obtain a black powder.

- The powder obtained in aforesaid step was ground and then heated in the furnace at 1000^{0}C for 8 hours.

2.3 X-RAY DIFFRACTION:

XRD is the most commonly used structural characterization technique for studying the powder form as well as thin film form samples. It is used to uniquely define the crystalline phases of the material, out of plane orientations of the thin film grain and relative in plane alignments of the thin film with the substrate or between different layers in the case of the heterostructures. In normal θ-2θ scan mode, a beam of monochromatic X-rays is incident on the sample, making an angle θ with the sample surface. The detector motion is coupled with that of X-ray source so that it is always kept at a position at an angle of 2θ with the incident direction of the X-ray beam. The schematic of X-ray diffractometer is shown in Fig.2.2.

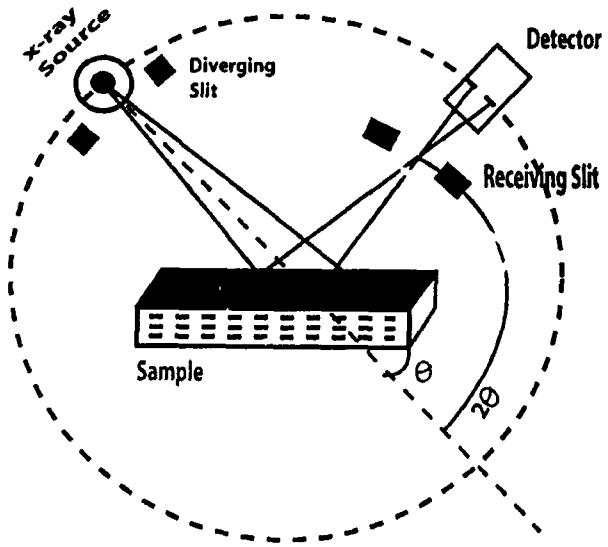

Fig.2.2 The schematic of X-ray diffractometer.

The recorded diffraction pattern gives the Intensity versus 2θ plot. The XRD patterns were recorded with diffractometer. XRD can provide additional information beyond basic identification. If the sample is a mixture, XRD data can be analyzed to determine the proportion of the different minerals present. Other information obtained can include the degree of crystallinity [8].

The X-rays get diffracted from the crystal planes when the Bragg condition is satisfied. The condition is given as;

$$2d \sin\theta = n\lambda \qquad (2.1)$$

where'd' is the interplaner spacing, 'n' is the order of diffraction, λ is the wave length of X-rays used and θ is the incident glancing angle. This equation puts very stringent conditions on λ and θ for any given crystal. In order to satisfy the Bragg law, either λ or θ can be varied and this is done in different diffraction methods as given in table-1;

Table-1

METHOD	ANGLE(θ)	WAVELENGTH OF X-RAY
LAUE-METHOD	Fixed	Variable
ROTATING CRYSTAL METHOD	Variable (in parts)	Fixed
POWDER METHOD	Variable	Fixed

The structural analysis is carried out using X-rays of known wavelength λ. By measuring 2θ, one can determine the spacing d between the planes in the crystal. The diffraction pattern gives us information about the particle/grain

size, lattice parameters, crystal structure of the samples etc. The positions in the unit cell affect the intensities but not the directions of the diffracted beams. The intensity of the diffracted beam is changed by any change in atomic positions; conversely the atomic positions can be determined by the observations of diffracted intensities. It is interesting to understand the complex problem of relation between the atomic position and diffracted intensity. By measuring the shift in the diffraction peak position one can get idea of the strain present in the sample.

The powder X-Ray diffraction patterns have been recorded for the series of $La_{1-x}Ca_xMnO_3$ (x=.25, .33, .40, .45, .50, .55, .60), $La_{1-x}Ba_xMnO_3$ (x=.10, .15, .20, .33, .45) and $La_{1-x}Sr_xMnO_3$ (x=.25, .33, .40, .50) using the XPERT-PRO X-Ray diffractometer with a Cu-source having radiation of wavelength 1.54060 Angstroms at room temperature. The cathode was maintained at 40 kV voltages. Diffraction patterns were recorded in the range $20^0 \leq 2\theta \leq 80^0$. The lattice parameters have been determined using powder X software. The indices could be assigned to all the lines on the basis of orthorhombic symmetry.

2.3.1 STRUCTURAL ANALYSIS OF THE X-RAY DATA:

Fig. 2.3 shows the general approach to the structural analysis using XRD data which has been employed in the present work.

The X-ray data has been recorded on an X-ray diffractometer at SAIF (Sophisticated Analytical Instrumentation Facility, Punjab University) using a Cu-source of wavelength 1.54060 angstroms. The analysis of the X-ray data has been done using various computer softwares. One of them used prominently in the present work is Powder-X [9]. We have used this software to obtain the unit cell parameters and FWHM (Full Width of Half Maximum).

2.3.1.1 Powder X

The features of Powder X can be summarized as:

1. Powder X can read 13 data formats, from either angular-dispersive or energy dispersive x-ray diffraction, used in various diffractometers made by Mac Science, Philips, Seimens, Rigaku etc. It can also write many data formats used for ab-initio structural solution and Reitveld refinements (EXPO, DBWS, GSAS, FULLPROF, RIETAN etc.)

2. It displays both the previous data and the data after processing so that it becomes very easy to see the effects of the processes during smoothening, background subtraction and 2 elimination.

3. It offers a simple method for parameters input and it makes easy to use interfaces.

4. It provides for various methods of data smoothening, 2 elimination and peak search are available, so that the user can find optimum method for his data set. The high-angle side fluctuation is less than 0.5% of the peak intensity in our method for Cu-K_2 elimination, which is much better than conventional Rachinger and Ladell methods.

5. Derivatives and Fourier transforms of the x-ray data can be calculated, plotted and saved as data files.

6. Zero shift and other geometrical aberrations can be easily calculated and corrected.

7. Any part of the plot can be zoomed with mouse to see the details.

8. It prints the ready-to-publish plots of x-ray diffraction data.

9. It edits the control file using graphical interfaces for pattern fitting programme Simpro.

10. Several other programmes, d_{hkl} (the calculation of diffraction angles and crystal plane spacings from lattice parameters), Lazy (generation of the simulated powder x-ray diffraction patterns), Treor90 (Index) and Eracel have been included in this system with user-friendly interfaces.

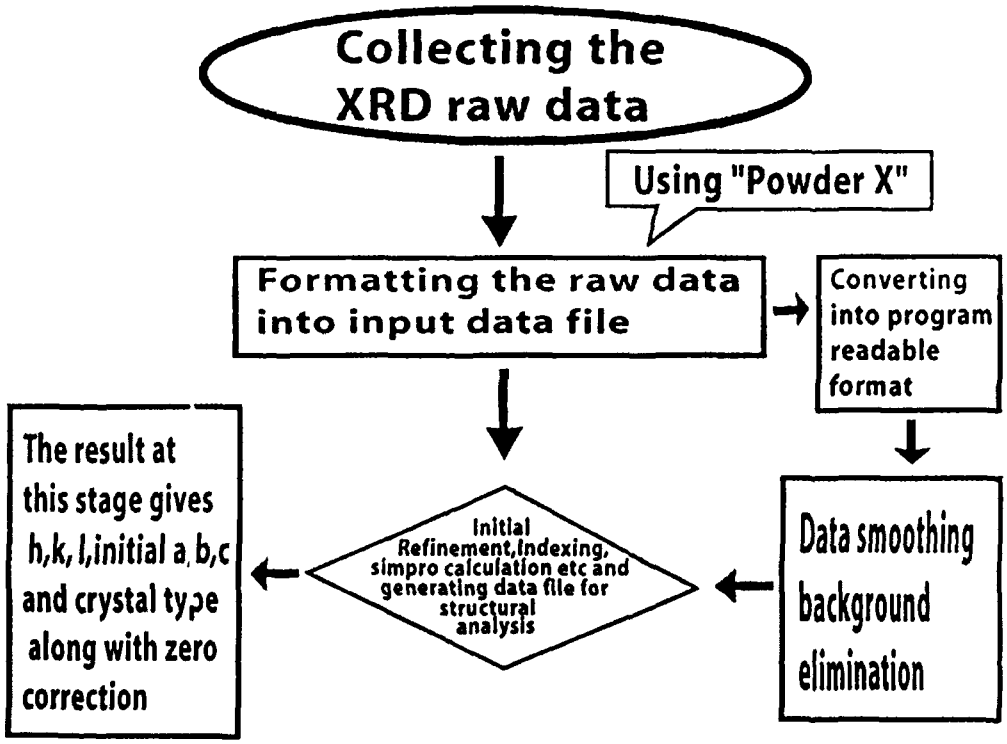

Fig.2.3 Block diagram for the structural analysis of XRD data using Powder- X.

2.4 DESCRIPTION OF FOUR-PROBE METHOD

Resistivity measurements of $La_{1-x}Sr_xMnO_3$ (x=.25, .33) prepared by both Solid-State reaction route and Sol-Gel method are carried out using standard four-probe technique in the temperature range (30K-300K) . These studies show that with the doping of Sr, the samples show the semiconducting behaviour. When the sample resistance is measured by two probes using a multimeter, the contact

and the lead wire resistances can not be avoided. The four-probe method is a simple technique to overcome this limitation.

Four contacts were made on a well sintered pellet using conductive solder of low melting point. Fine enamelled copper wires were used to pass the constant current of the order of few microamperes through the outer two leads using a constant current source (KEITHLY, Model-6220). The voltage developed across the two inner leads was measured using the multimeter (KEITHLY-2000) as a function of temperature. The resistivity as a function of temperature was measured during the warming up cycle. The block diagram of the four-probe set up used for measuring the resistivity is shown in Fig. 2.4;

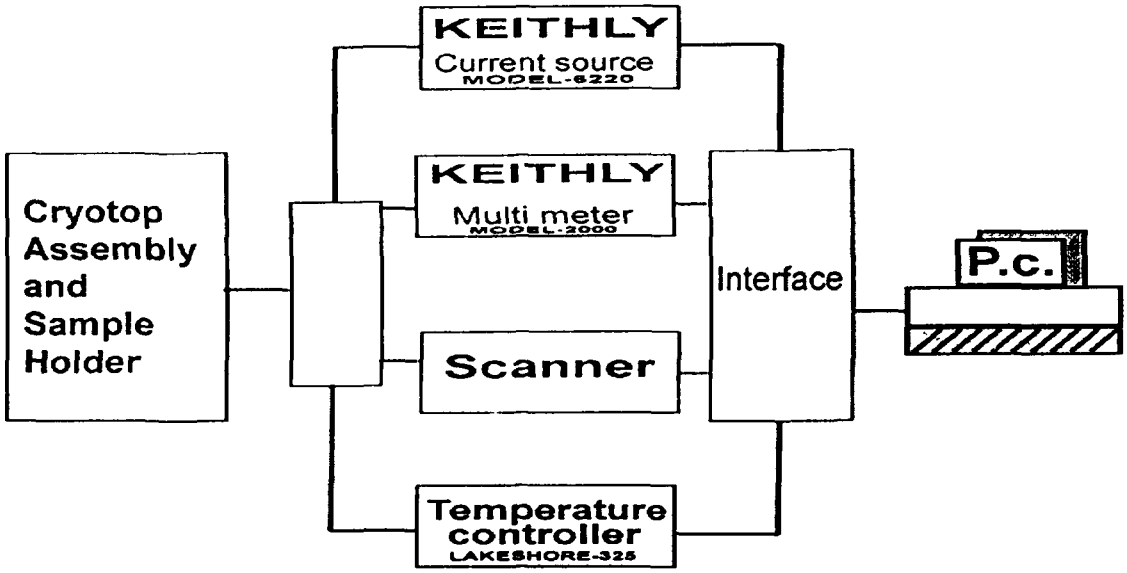

Fig. 2.4 Block diagram of four-probe resistivity set-up.

2.5 DESCRIPTION OF VIBRATING SAMPLE MAGNETOMETER (VSM):

The vibrating sample magnetometer has become a widely used instrument for determining magnetic properties of a large variety of materials: diamagnetics, paramagnetics, ferromagnetics, ferromagnetics and antiferromagnetics. This

experimental technique was invented in 1956 by Simon Foner, a scientist of the MIT.

It has a flexible design and combines high sensitivity with easy of sample mounting and exchange. Samples may be interchange rapidly even at any operating temperature. Measurements of magnetic moments as small as $5x10^{-5}$ emu are possible in magnetic fields from zero to 9 Tesla (or higher). Maximum applied fields of 2-3 Tesla or 9 Tesla are reached using conventional laboratory electromagnets and superconducting solenoids, respectively. Vibrating sample magnetometers normally operate over a temperature range of 2.0 to 1050 K. Powders, bulk and thin films can be measured and studied.

PRINCIPLE: - If a sample of any material is placed in a uniform magnetic field, created between the poles of an electromagnet, a dipole moment will be induced. If the sample vibrates with sinusoidal motion, a sinusoidal electrical signal can be induced in suitable placed pick-up coils.

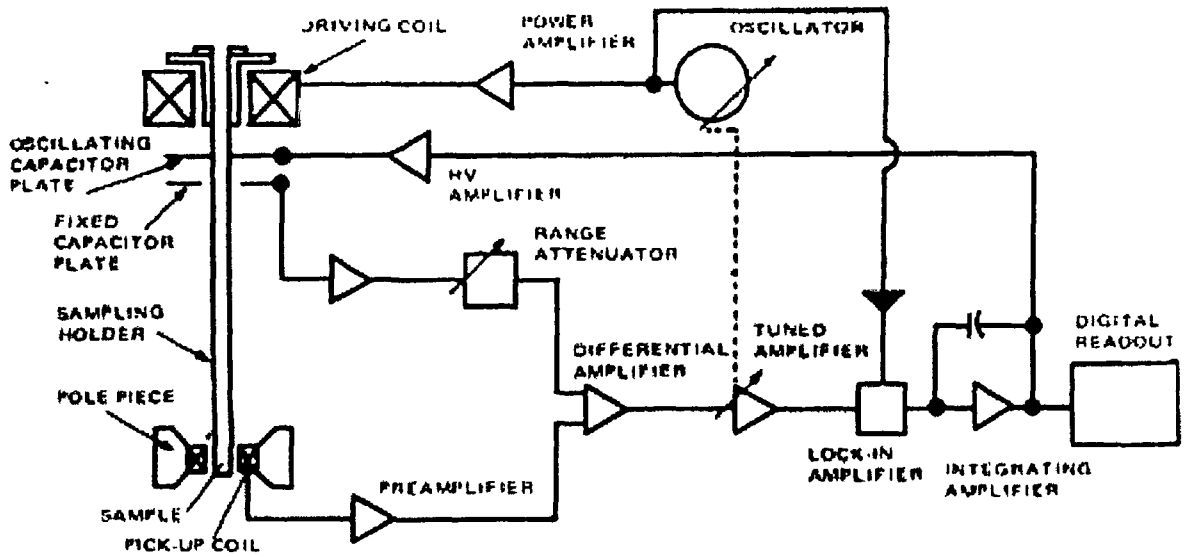

Fig. 2.5 Block-diagram of Vibrating Sample Magnetometer.

The signal has the same frequency of vibration and its amplitude will be proportional to the magnetic moment, amplitude, and relative position with respect to the pick-up coils system. The Fig. 2.5 shows the block-diagram of Vibrating Sample Magnetometer. The sample is fixed to a small sample holder located at the end of a sample rod mounted in a electromechanical transducer. The transducer is driven by a power amplifier which itself is driven by an oscillator at a frequency of 90 Hertz. So, the sample vibrates along the Z-axis perpendicular to the magnetizing field. The latter induced a signal in the pick-up coil system that is fed to a differential amplifier. The output of the differential amplifier is subsequently fed into a tuned amplifier and an internal lock-in amplifier that receives a reference signal supplied by the oscillator. The output of this lock-in amplifier, or the output of the magnetometer itself, is a DC signal proportional to the magnetic moment of the sample being studied. The electromechanical transducer can move along X, Y and Z directions in order to find the saddle point (which Calibration of the vibrating sample magnetometer is done by measuring the signal of a pure Ni standard of known the saturation magnetic moment placed in the saddle point.

The basic instrument includes the electromechanical system and the electronic system (including a personal computer), while the costumer should select the electromagnet or superconducting coil system with the appropriate bipolar power supply. Laboratory electromagnets or superconducting coils of various maximum field strengths may be used. For ultra-high magnetic fields a cryogen-free magnets can be also used. For the characterization of soft magnetic materials a pair of Helmholtz coils may also be used.

REFERENCES

1. G.H. Jonker and J.H. van Santen, Physica **16** (1950) 337
2. P. Schiffer, A.P. Ramirez, W. Bao and S.W. Cheong, Phys. Rev. Lett. **75** (1995) 3336
3. S.B. Ogale, R. Shreekala, Ravi Bathe, S.K. Date, S.I. Patil, B. Hannoyer, F. Patit and G. Marest, Phys. Rev. B **57** (1998) 7841
4. P. Mandal and S. Das, Phys. Rev. B **56** (1997) 15073
5. R.D. Sanchez, J. Rivas, C. Vazquez-Vazquez, A. Lopez-Quintela, M.T. Causa, M. Tovar and S. Oseroff, Appl. Phys. Lett. **68** (1996) 1334
6. P. Barboux, J.M. Tarascon, L.H. Greene, G.W. Hull, B.G. Bagley, J. Appl. Phys. **63** (1988) 2725
7. X.Z. Wang, M. Henry, J. Livage, Solid State Comm. **64** (1987) 881
8. M. Phil. Dissertation; Dr. M. Wasi Khan, Physics Department, AMU, Aligarh
9. *Elements of X-ray Diffraction*, ed. by B.D. Cullity (Addison Wesley Publ. Co., 1978).
10. C. Dong, J. Appl. Cryst. **32** (1999) 838

CHAPTER-3

RESULTS AND DISCUSSIONS

3.1 INTRODUCTION:

In this chapter we discuss the interpretation of our studies on the structural properties of $La_{1-x}Sr_xMnO_3$ (x=0.25, 0.33, 0.40, 0.50), prepared by both Solid-State reaction route and Sol-Gel method. The powder x-ray diffraction (XRD) pattern of the whole series of $La_{1-x}Sr_xMnO_3$ has been recorded at room temperature. The lattice parameters and the unit cell volume of all the samples have been calculated.

Also, this chapter deals with the electrical and magnetic properties of Sr doped $LaMnO_3$ in bulk forms. The temperature dependence of electrical resistivity has been measured for different Sr concentration samples down to liquid nitrogen temperature to determine the metal-insulator transition temperature (MIT).

3.2 THE STRUCTURAL ANALYSIS (BULK SAMPLES):

The analysis of powder XRD patterns of the samples prepared by conventional Solid-State reaction route and Sol-Gel method are shown in Figs. 3.1(a), 3.1(b), 3.1(c), 3.1(d) and in Figs. 3.2(a), 3.2(b), 3.2(c) respectively. At room temperature, the XRD patterns show that all the samples formed in the single phase structure with the orthorhombic crystal symmetry. The lattice parameters of $LaMnO_3$ change considerably with Sr doping. The unit cell volume fluctuates (sometimes increases and sometimes decreases) with increase in the Sr concentration, obviously due to size mismatch of La and Sr ions. We summarize all these observations in Table 3.1 and Table 3.2 respectively.

Also, the particle size of different compositions of $La_{1-x}Sr_xMnO_3$ is tabulated in Table 3.3 and Table 3.4 and it is observed that they all are almost same for Solid-State Reaction Route and Sol-Gel method.

TABLE 3.1 THE LATTICE PARAMETERS AND THE UNIT CELL VOLUME FOR DIFFERENT COMPOSITIONS OF $La_{1-x}Sr_xMnO_3$ (SOLID-STATE REACTION-ROUTE):

COMPOSITION	CRYSTAL SYMMETRY	a (Å)	b (Å)	c (Å)	UNIT CELL VOL.(Å^3)
$LaMnO_3$	Orthorhombic	5.582	5.515	7.763	238.982
$La_{0.75}Sr_{0.25}MnO_3$	Orthorhombic	5.602	5.607	7.770	244.058
$La_{0.67}Sr_{0.33}MnO_3$	Orthorhombic	5.440	5.490	7.740	231.159
$La_{0.60}Sr_{0.40}MnO_3$	Orthorhombic	5.551	5.604	7.760	241.396
$La_{0.50}Sr_{0.50}MnO_3$	Orthorhombic	5.429	5.468	7.745	229.916

TABLE 3.2 THE LATTICE PARAMETERS AND THE UNIT CELL VOLUME FOR DIFFERENT COMPOSITIONS OF $La_{1-x}Sr_xMnO_3$ (SOL-GEL METHOD):

COMPOSITION	CRYSTAL SYMMETRY	a (Å)	b (Å)	c (Å)	UNIT CELL VOL. ($Å^3$)
$LaMnO_3$	Orthorhombic	5.582	5.515	7.763	238.982
$La_{0.75}Sr_{0.25}MnO_3$	Orthorhombic	5.602	5.617	7.770	244.494
$La_{0.67}Sr_{0.33}MnO_3$	Orthorhombic	5.420	5.480	7.740	229.890
$La_{0.60}Sr_{0.40}MnO_3$	Orthorhombic	5.541	5.600	7.730	239.858

TABLE 3.3 PARTICLE SIZE FOR DIFFERENT COMPOSITIONS OF $La_{1-x}Sr_xMnO_3$:

(SOLID-STATE REACTION-ROUTE):

Compositions	Particle Size (nm)
$La_{0.75}Sr_{0.25}MnO_3$	19.06
$La_{0.67}Sr_{0.33}MnO_3$	21.60
$La_{0.60}Sr_{0.40}MnO_3$	21.08
$La_{0.50}Sr_{0.50}MnO_3$	20.97

TABLE 3.4 PARTICLE SIZE FOR DIFFERENT COMPOSITIONS OF $La_{1-x}Sr_xMnO_3$:

(SOL-GEL METHOD):

Compositions	Particle Size (nm)
$La_{0.75}Sr_{0.25}MnO_3$	21.58
$La_{0.67}Sr_{0.33}MnO_3$	22.08
$La_{0.60}Sr_{0.40}MnO_3$	20.44

As reported in literature, under similar conditions for similar compositions, the divalent cation doped $LaMnO_3$ shows the cubic symmetry. But the Sr doped $LaMnO_3$ shows the orthorhombic symmetry. This may be due to the valence fluctuation and the size differences in the A sublattice ions in $La_{1-x}Sr_xMnO_3$ compounds.

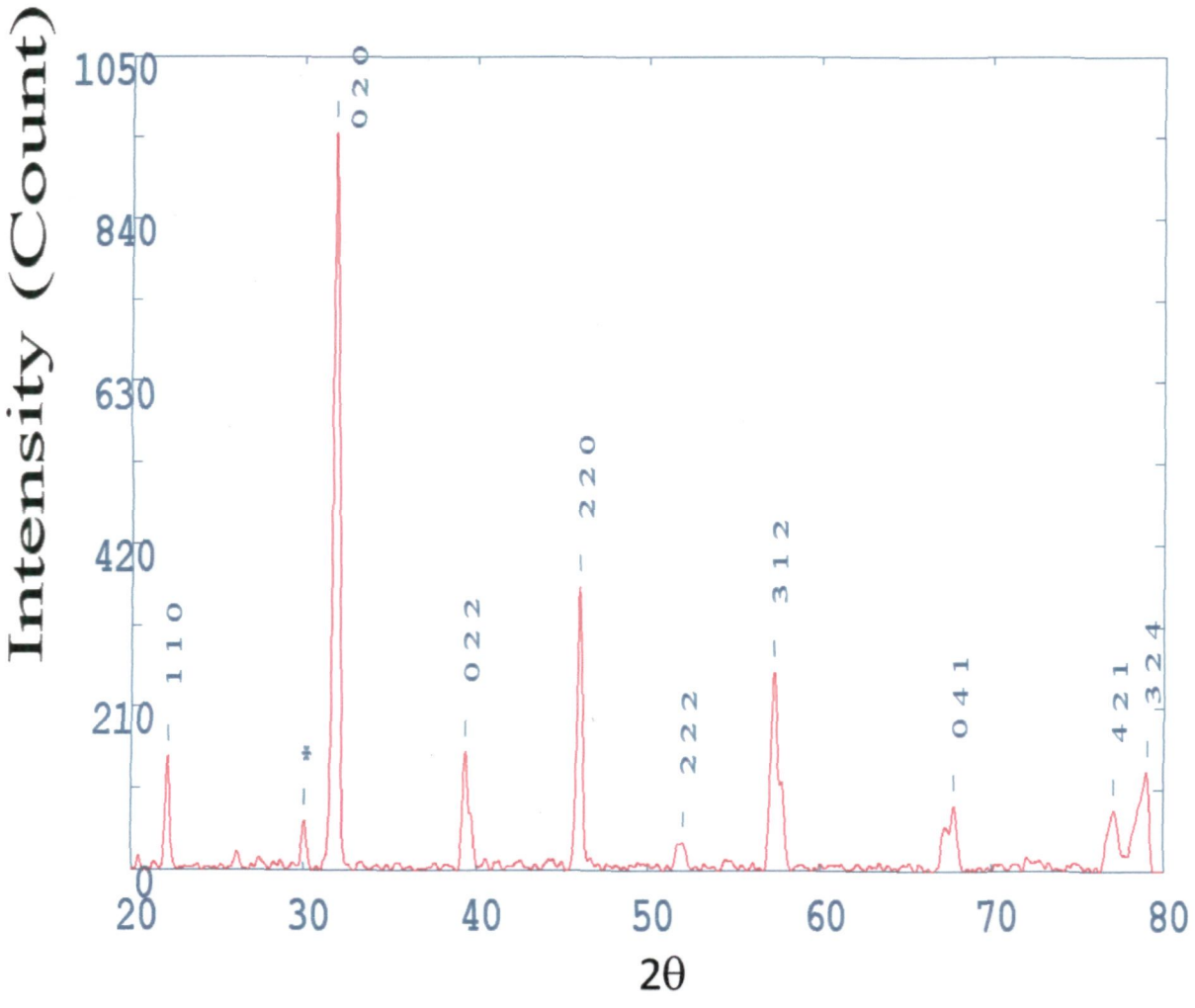

Fig. 3.1(a) XRD pattern of LSMO (SSRR) with x = 0.25*

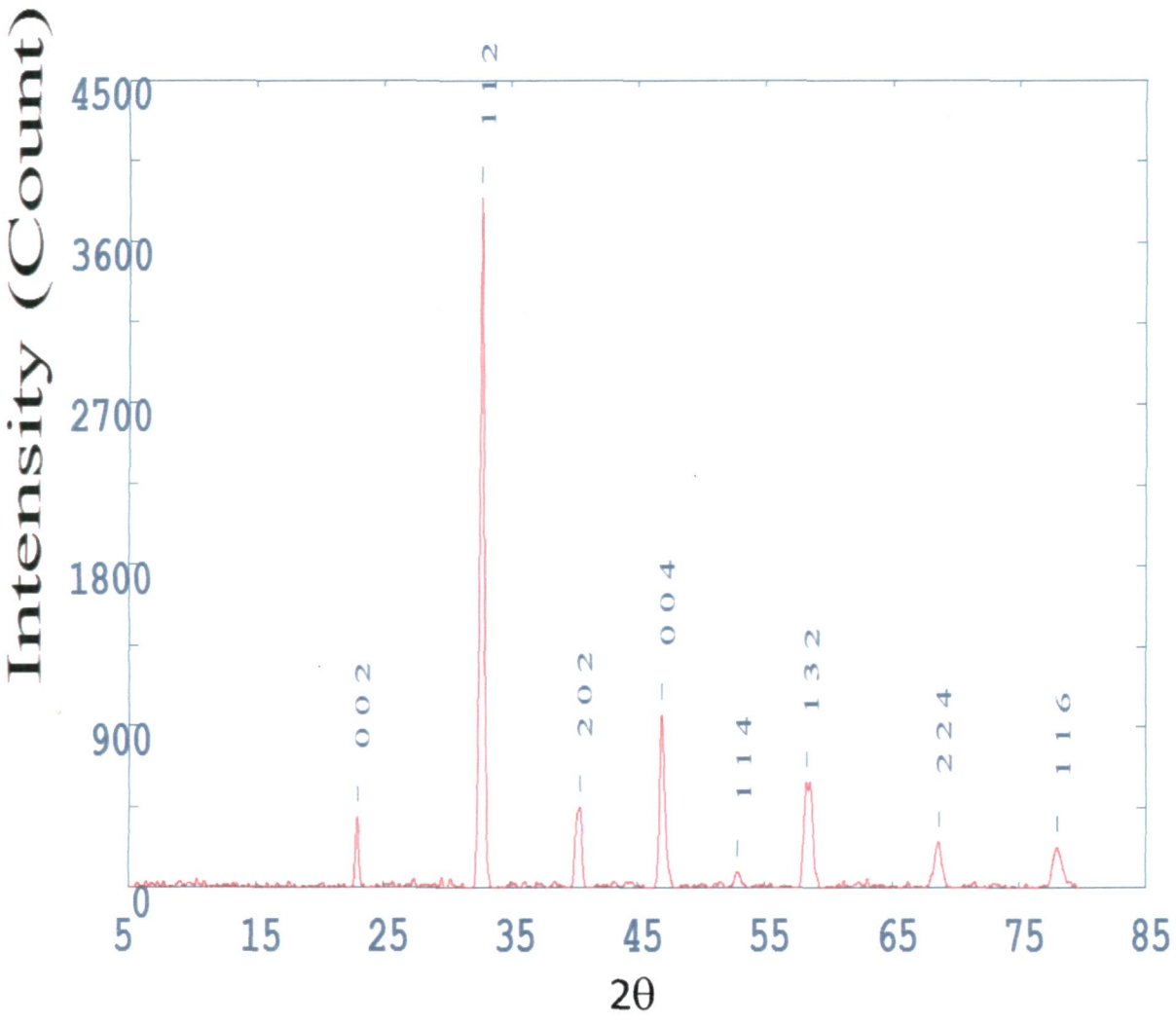

Fig. 3.1(a) XRD pattern of LSMO (SSRR) with x = 0.33*

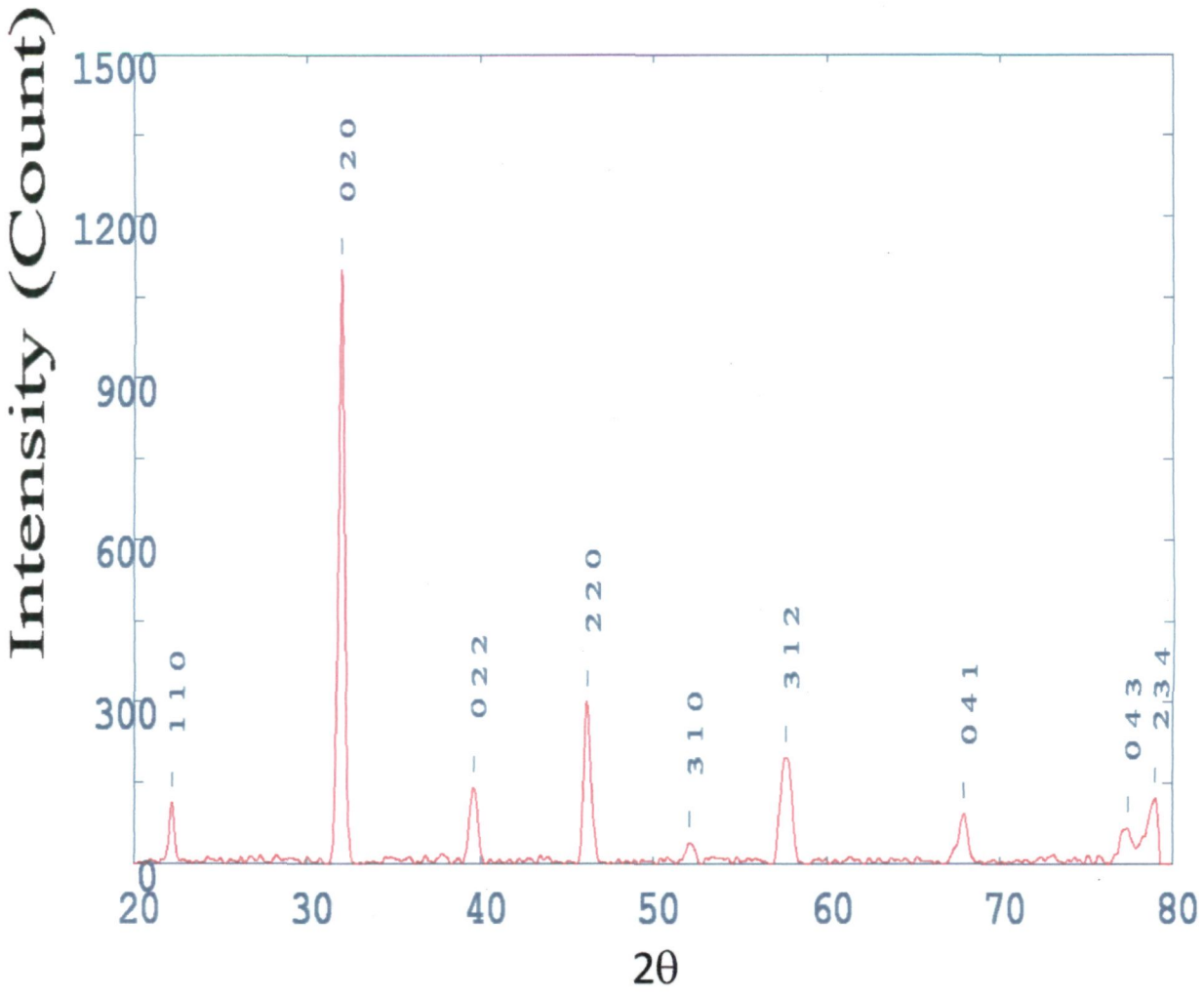

Fig. 3.1 (c) XRD pattern of LSMO (SSRR) with x = 0.40*

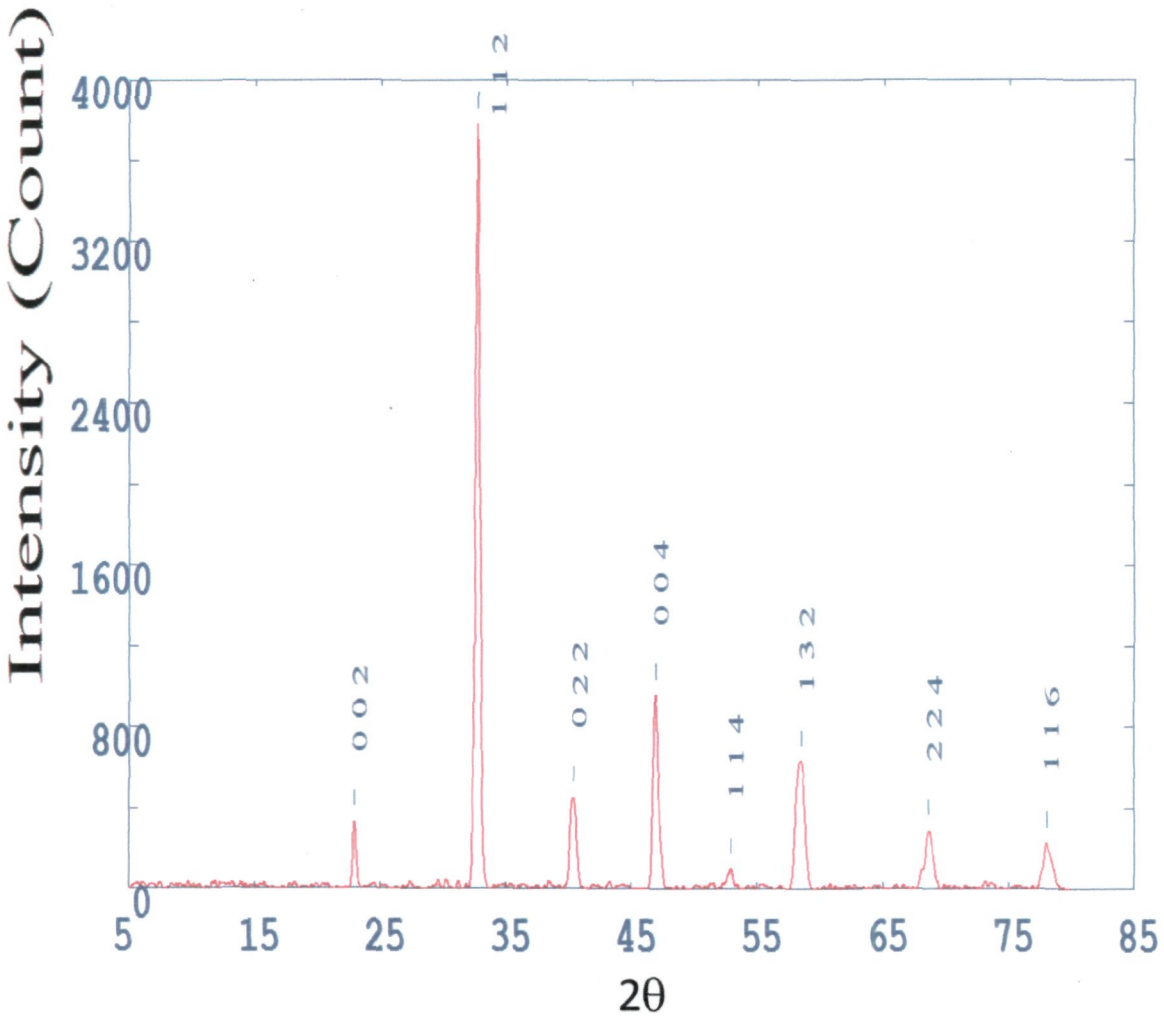

Fig. 3.1 (d) XRD pattern of LSMO (SSRR) with x = 0.50.*

**For Solid-State Reaction Route.*

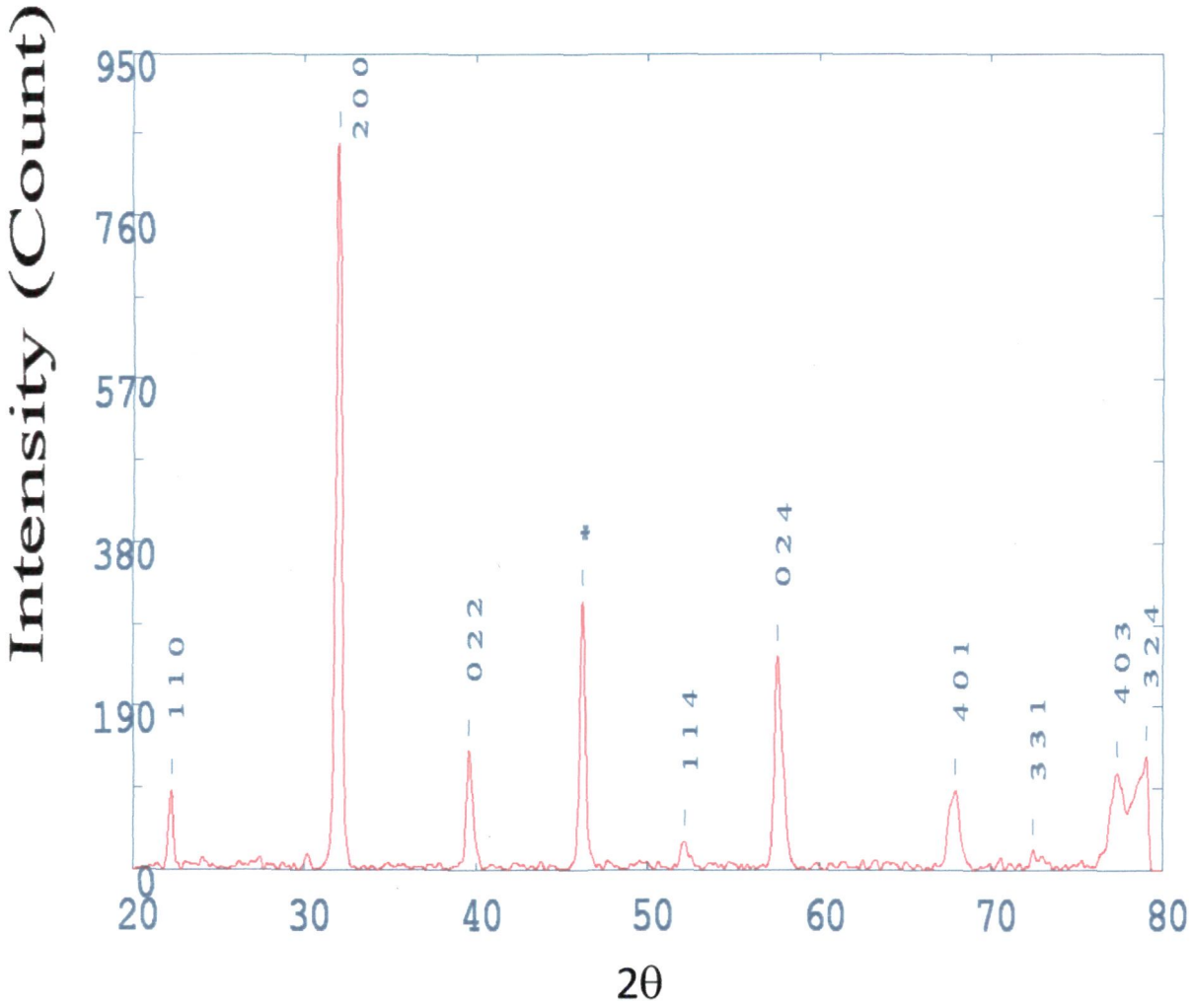

Fig. 3.2 (a) XRD pattern for LSMO (SGM) with x = 0.25*

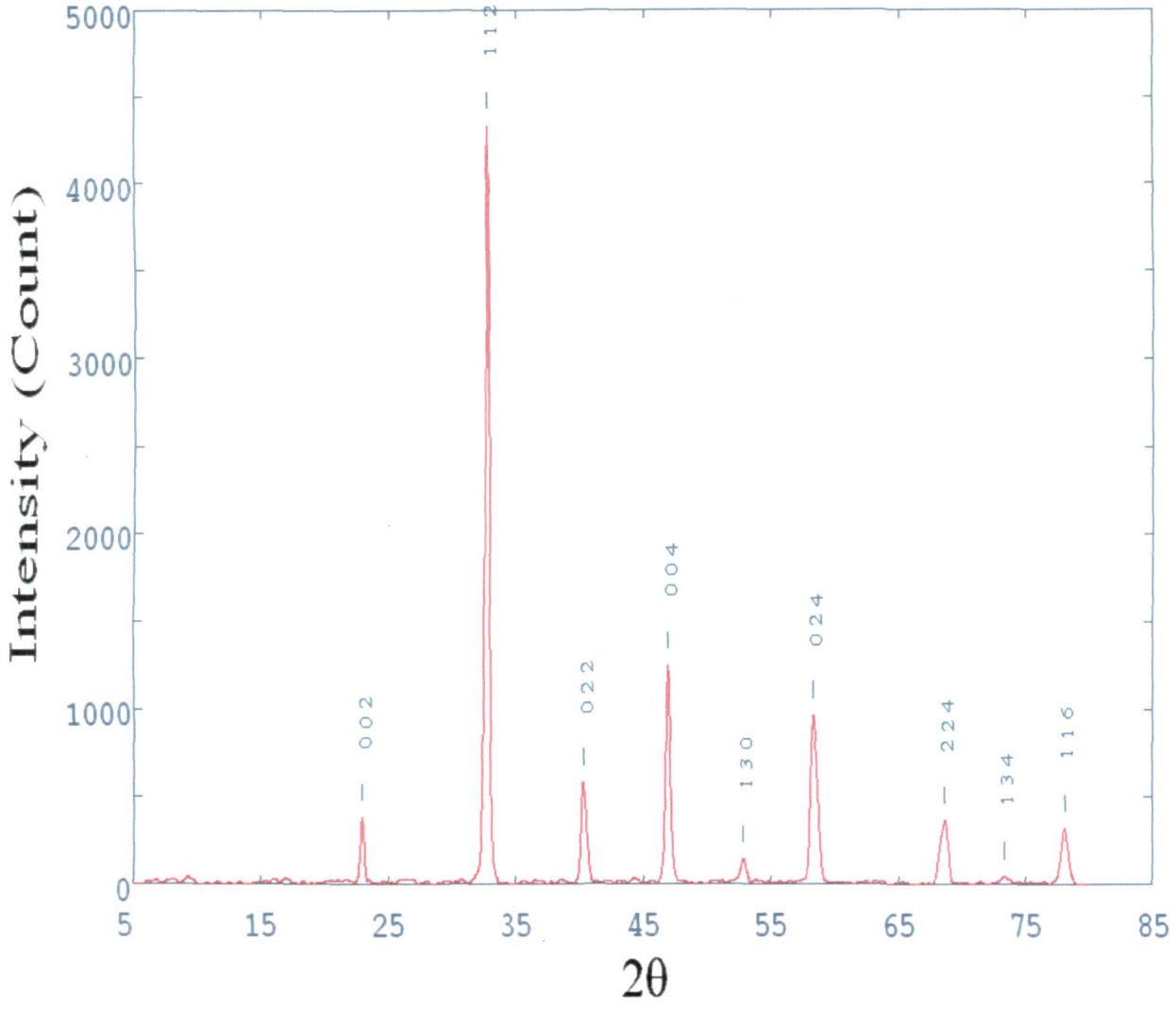

Fig. 3.2 (b) XRD pattern for LSMO (SGM) with x= 0.33*

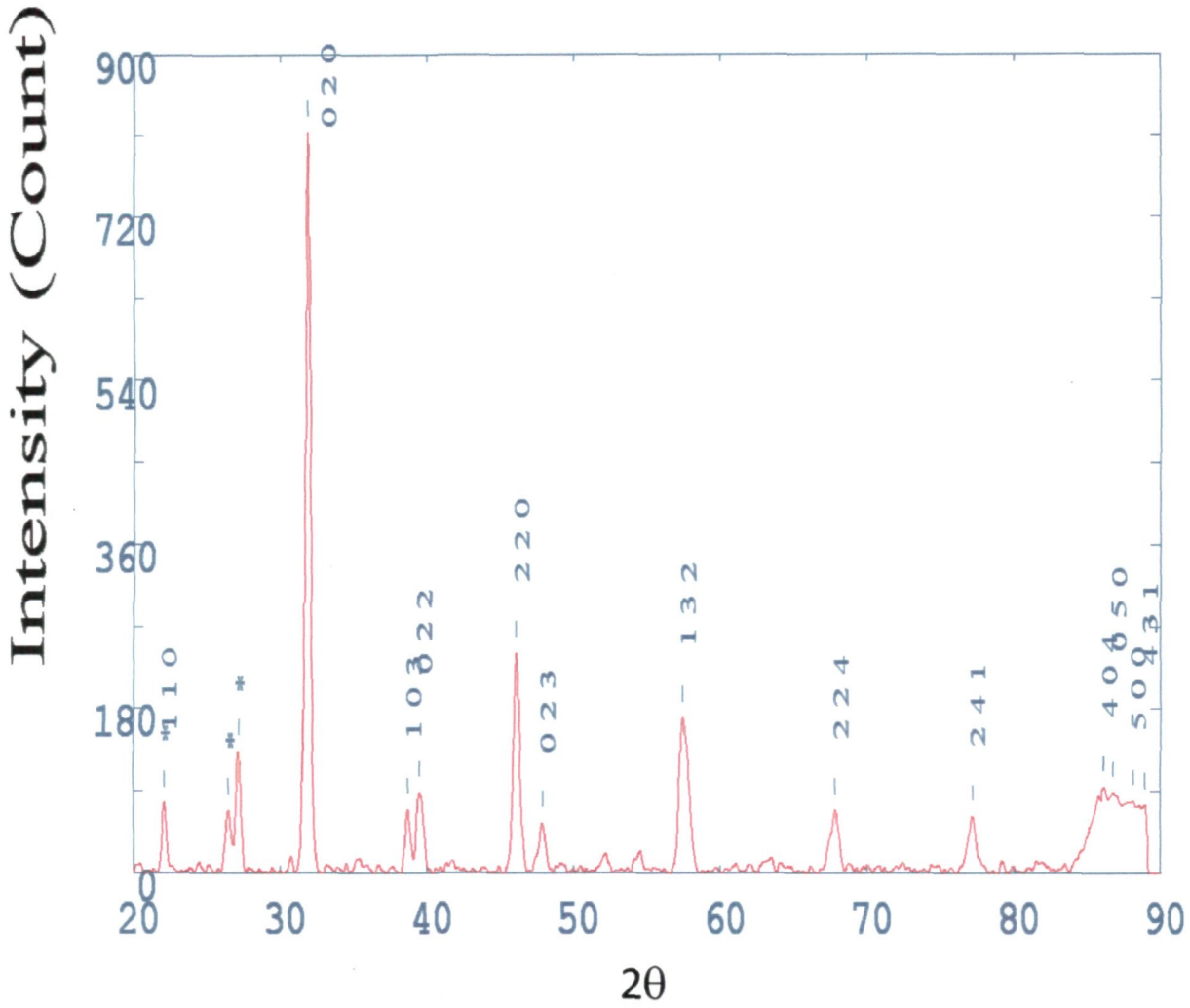

Fig. 3.2 (c) XRD patterns for LSMO (SGM) with x= 0.40*

** For Sol-Gel Method.*

3.3 TRANSPORT ANALYSIS:

Figs. 3.3(a), 3.3(b) show the temperature dependence of resistivity for $La_{1-x}Sr_xMnO_3$ (x = 0.25) and $La_{1-x}Sr_xMnO_3$ (x = 0.33) prepared by Solid-State reaction route and Sol-Gel method respectively. All the samples show metal-

insulator transition (MIT). In Fig. 3.3 (a), the values of metal-insulator transition temperatures are respectively 168.42 K and 135.20 K and in Fig. 3.3 (b), the value of metal-insulator transition temperatures are respectively 136.39 K and 215.20 K, which are slightly different with earlier reported results. All the transition temperatures are far away from the room temperature.

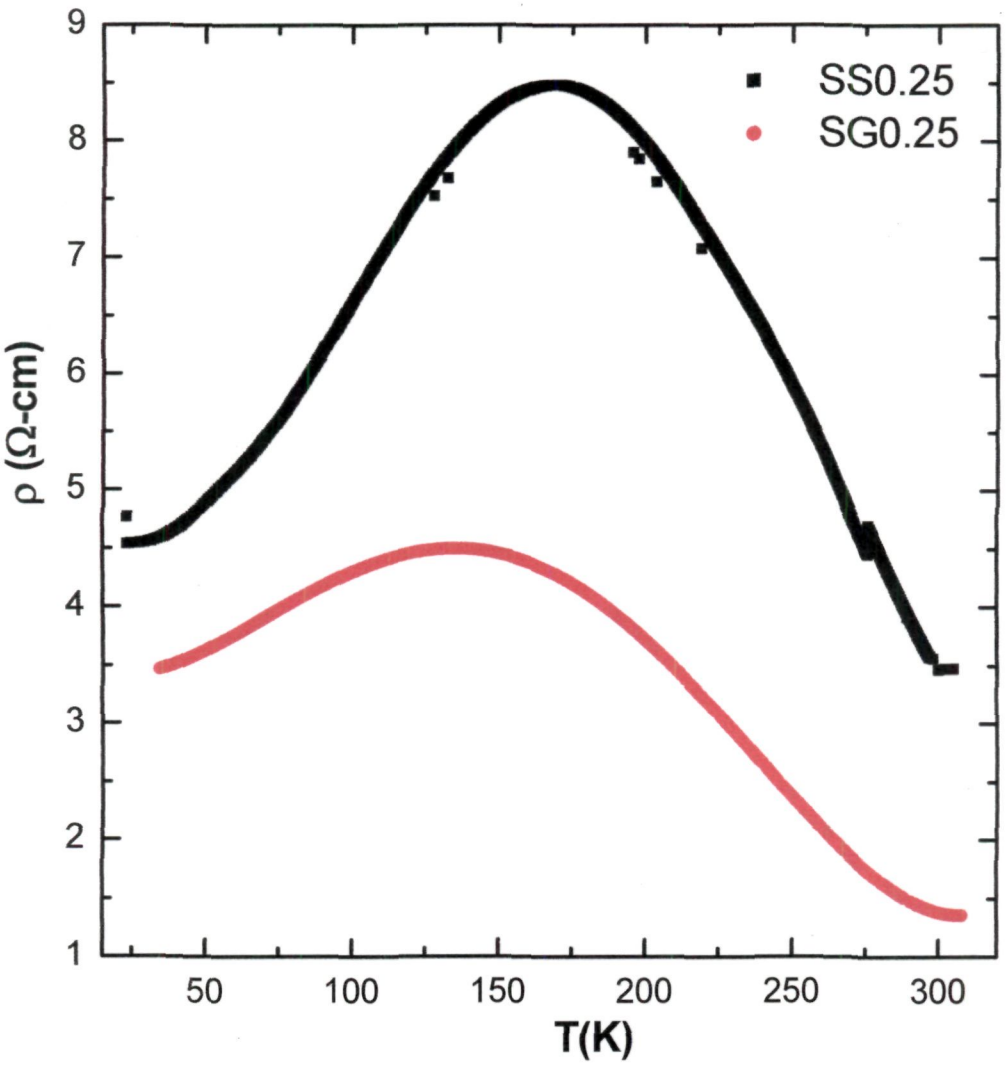

Fig. 3.3 (a) Temperature dependence of Resistivity for LSMO (x = 0.25).

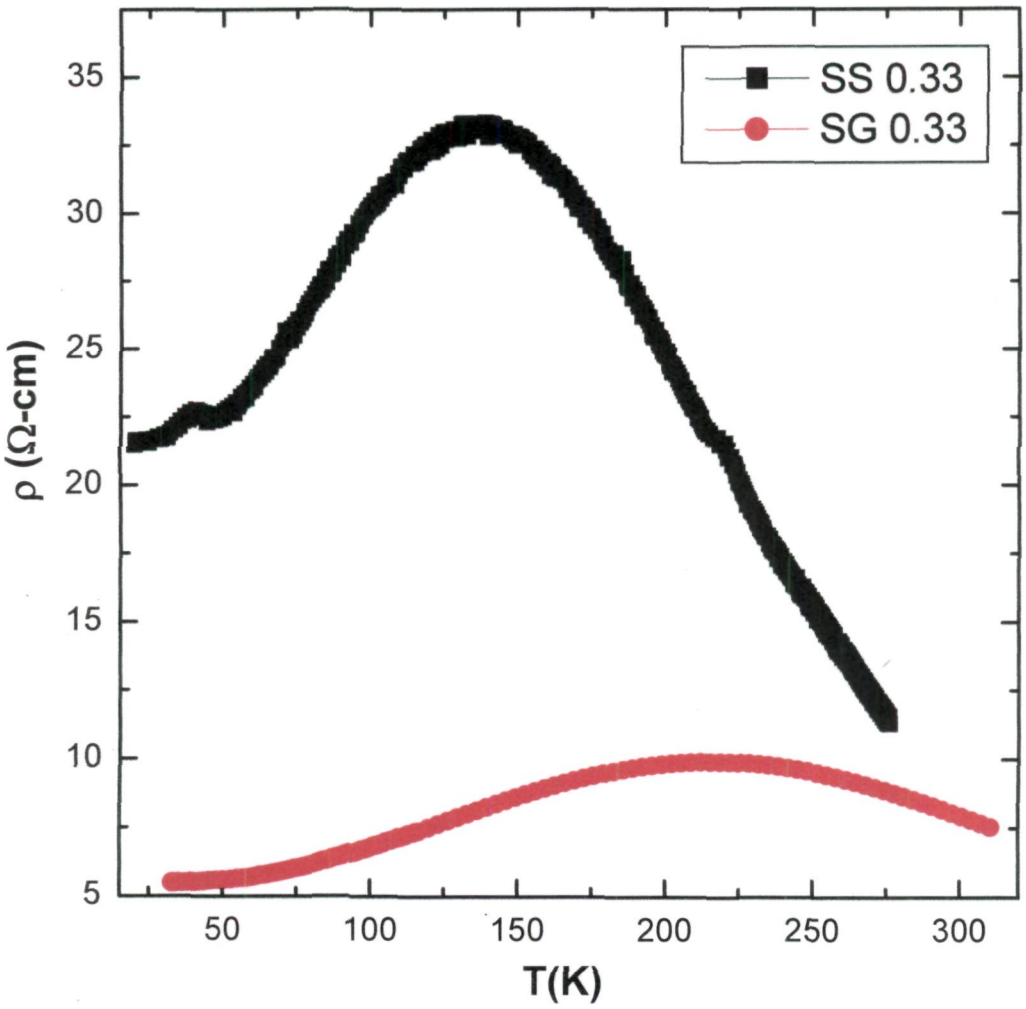

Fig. 3.3 (b) Temperature dependence of Resistivity for LSMO (x = 0.33).

3.4 STRUCTURE AND ELECTRICAL ACTIVITY OF STRONTIUM:

It is known that for stoichiometric compositions of $LaMnO_3$, all manganese ions have Mn^{3+} charge states. Substitution of Sr^{2+} ions produces the formation of Mn^{4+} ions [1, 2, 3]. Within the limits of amorphous phase existence, the concentration of Mn^{4+} ions varies noticeably which characterizes a change in the electrical activity of strontium. In the process of atomic ordering at 100^0C, the activity of Sr is minimal which corresponds to the classical behaviour of an impurity in amorphous and glassy semiconductors [4]. When all impurity atoms saturate their valence bonds and form close electronic configurations; creating

neither acceptor nor donor states. The behaviour of Sr is one of the indications of a difference in the short range orders of the amorphous and crystalline states of La-Sr-MnO.

In manganese oxides such as $La_{1-x}Sr_xMnO_3$, manganese ions with different charge states i.e. Mn^{2+}, Mn^{3+}, and Mn^{4+} can co-exist [2]. The reason for the appearance of Mn^{2+} ions consists of the presence of local stresses stimulating the reaction;

$$2Mn^{3+} \longrightarrow Mn^{2+} + Mn^{4+}$$

According to the x-ray data, the change in resistivity is caused by the transition from mesoscopic order to long range atomic order, from the amorphous state of structure to the crystalline state. Thus impurity atoms of Sr become electrically active, creating Mn^{4+} ions directly in the structure of solid-solution [5].

3.5 LOW TEMPERATURE BEHAVIOR ($T<T_P$):

The relative strengths of the different scattering mechanisms originating from different contributions to the resistivity have been investigated by fitting the resistivity data at $T<T_P$ to various empirical equations [6, 7-9]. It has been concluded that the electrical resistivity data of the samples of the present investigation are found to fit well with the equation;

$$\rho = \rho_0 + \rho_2 T^2 + \rho_{4.5} T^{4.5} \qquad (3.1)$$

where ρ_0 arises due to the grain or domain boundary scattering [8, 9]. As the polycrystalline materials contain grain boundaries, their significant contribution to the resistivity is proved [10] and hence the term ρ_0 plays a major role in the conduction process. On the other hand, $\rho_2 T^2$ term explains the contribution of electron-electron scattering process to the resistivity, while the

term $\rho_{4.5}T^{4.5}$ may be attributed to two-magnon scattering process in the ferromagnetic region [11]. As a matter of fact, it was concluded that the magnon scattering process is more favourable in half-metallic band structured materials such as manganites [12]. The typical plots of resistivity versus temperature of LSMO (x= 0.25, 0.33), prepared by Solid-State Reaction-Route are shown in Figs. 3.4 (a) and 3.4 (b), and of LSMO (x = 0.25, 0.33) prepared by Sol-Gel method are shown in Figs. 3.4 (c) and 3.4 (d) respectively.

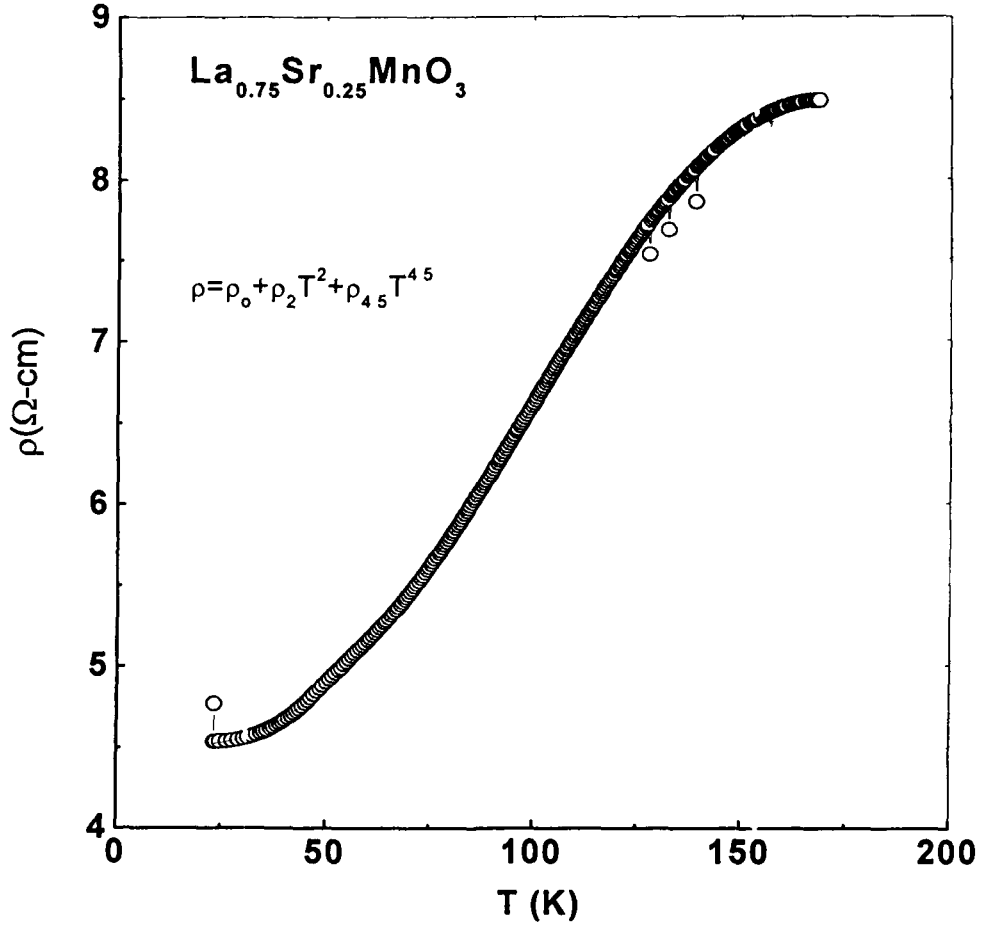

Fig. 3.4 (a) Low Temperature dependence of Resistivity of $La_{0.75}Sr_{0.25}MnO_3$.

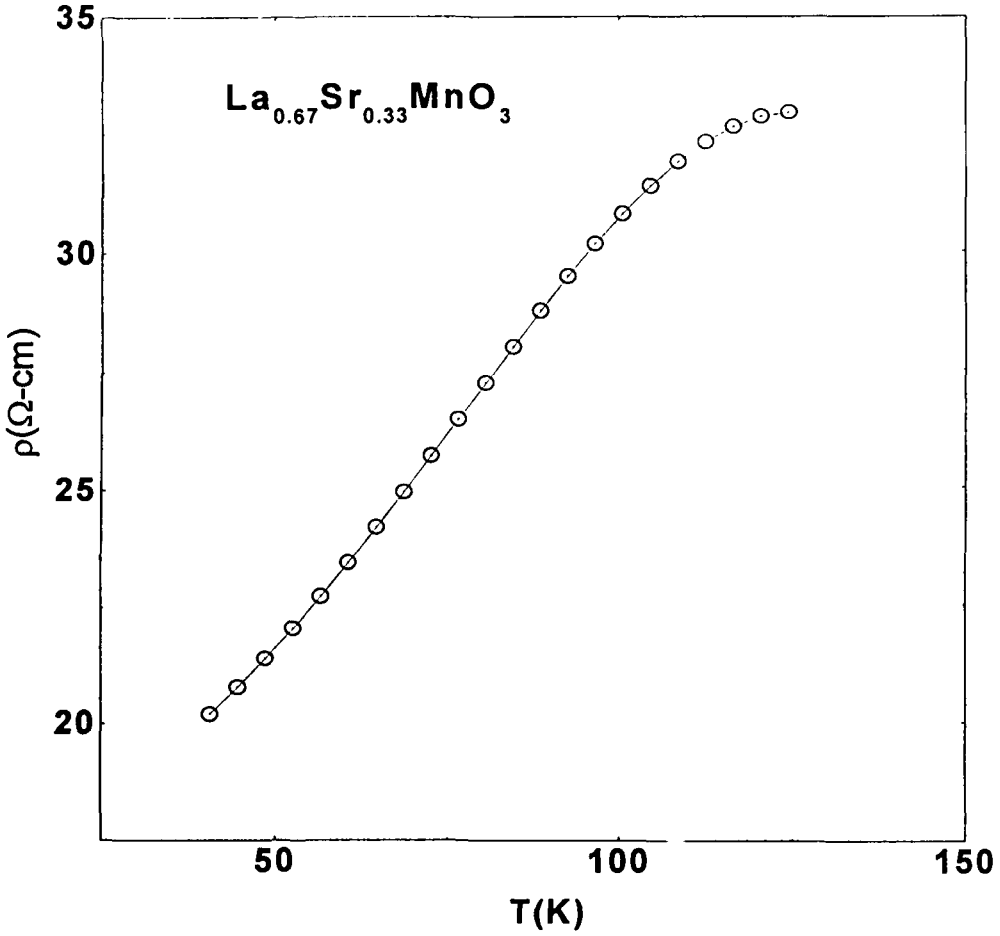

Fig. 3.4 (b) Low Temperature dependence of Resistivity for $La_{0.67}Sr_{0.33}MnO_3$.

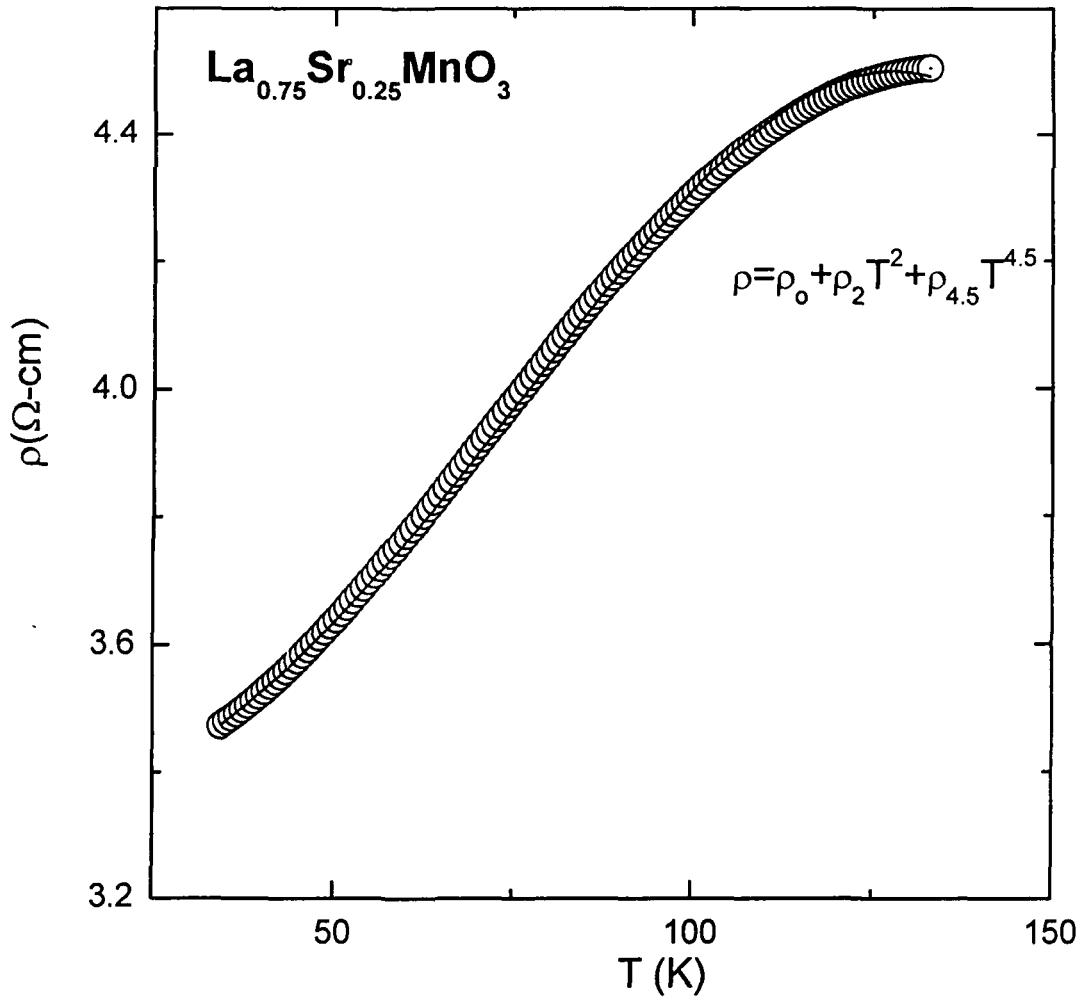

Fig. 3.4 (c) Low Temperature dependence of Resistivity for $La_{0.75}Sr_{0.25}MnO_3$.

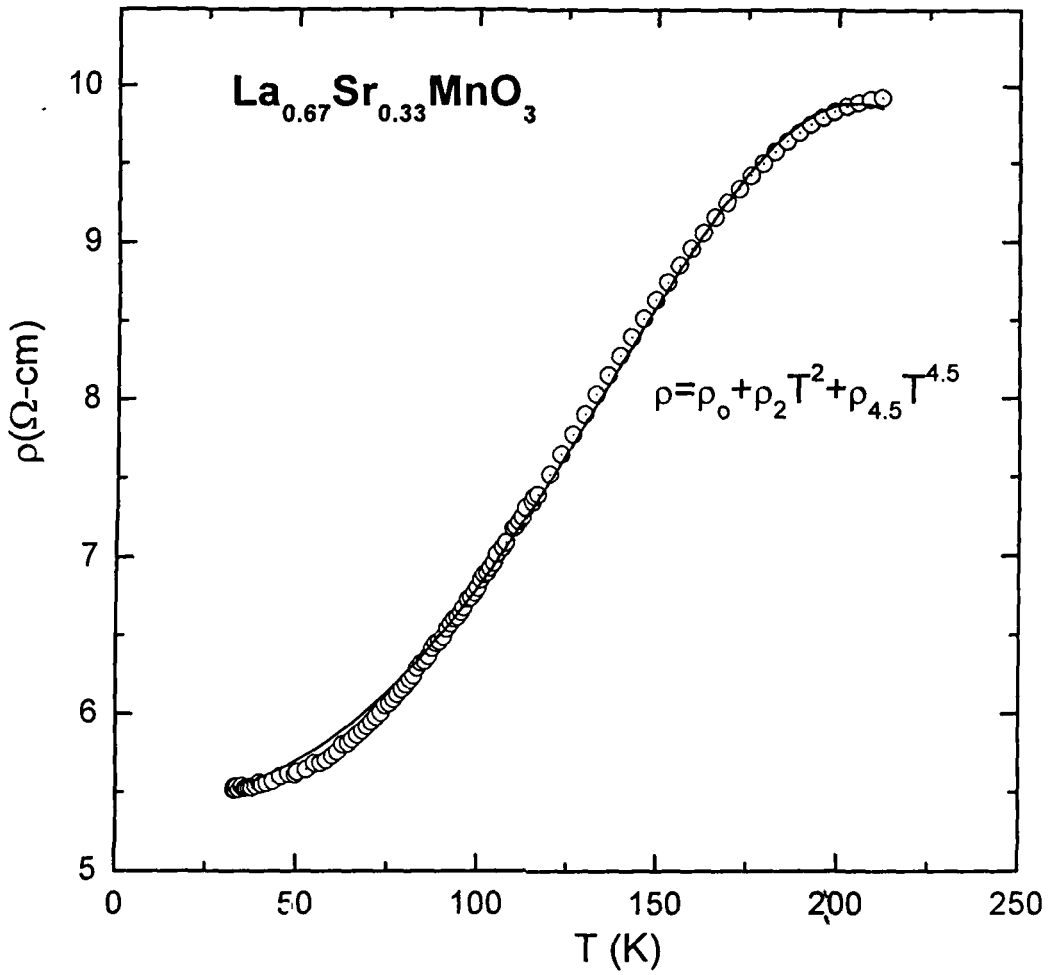

Fig. 3.4 (d) Low Temperature dependence of Resistivity for $La_{0.67}Sr_{0.33}MnO_3$.

The typical values of ρ_0, ρ_2 and $\rho_{4.5}$ for different compositions of $La_{1-x}Sr_xMnO_3$ are given in Table 3.5.

TABLE 3.5 RESISTIVITY COEFFICIENTS ρ_0, ρ_2 and $\rho_{4.5}$ FOR DIFFERENT COMPOSITIONS OF $La_{1-x}Sr_xMnO_3$:

COMPOSITIONS	ρ_0 (Ω-cm)	ρ_2(Ω -cm/K^2)	$\rho_{4.5}$(Ω-cm/K$^{4.5}$)
$La_{0.75}Sr_{0.25}MnO$*	4.51±0.0034	$-3.73\times10^{-10}\pm1.783\times10^{-12}$	1.52±0.00341
$La_{0.67}Sr_{0.33}MnO$*	17.30±0.0625	0.0018±0	$-4.57\times10^{-9}\pm0$
$La_{0.75}Sr_{0.25}MnO$#	3.32±0.0008	0.00013±0	$-3.13110\times10^{-10}\pm0$
$La_{0.67}Sr_{0.33}MnO$#	5.44±0	$1\times10^{-5}\pm6.59\times10^{-10}$	$-1.24\times10^{-11}\pm1.3754\times10^{-13}$

* Solid-State Reaction-Route. # Sol-Gel Method.

3.6 HIGH TEMPERATURE BEHAVIOR ($T>T_P$):

In the manganite systems at high temperature the lattice becomes distorted around the electrons in conduction band and due to the strong electron-phonon interaction small polarons are formed. Above the transition temperature (T_P), the thermally activated hopping of these polarons plays an important role. In the adiabatic approximation a small polaron hopping theory was proposed [13-15], according to which the activated conduction follows the relation:

$$\rho\,(T) = \rho_0 T \exp(E_a/k_B T) \qquad (3.2)$$

where k_B is Boltzmann constant, ρ_0 the resistivity coefficient and E_a is the activation energy. We fitted the high temperature resistivity data using the above relation for $La_{0.75}Sr_{0.25}MnO_3$ and $La_{0.67}Sr_{0.33}MnO_3$, prepared by Solid-State reaction route as shown in Fig. 3.5 (a) and 3.5 (b), and for $La_{0.75}Sr_{0.25}MnO_3$ and $La_{0.67}Sr_{0.33}MnO_3$, prepared by Sol-Gel method as shown in Fig. 3.5 (c) and 3.5 (d).

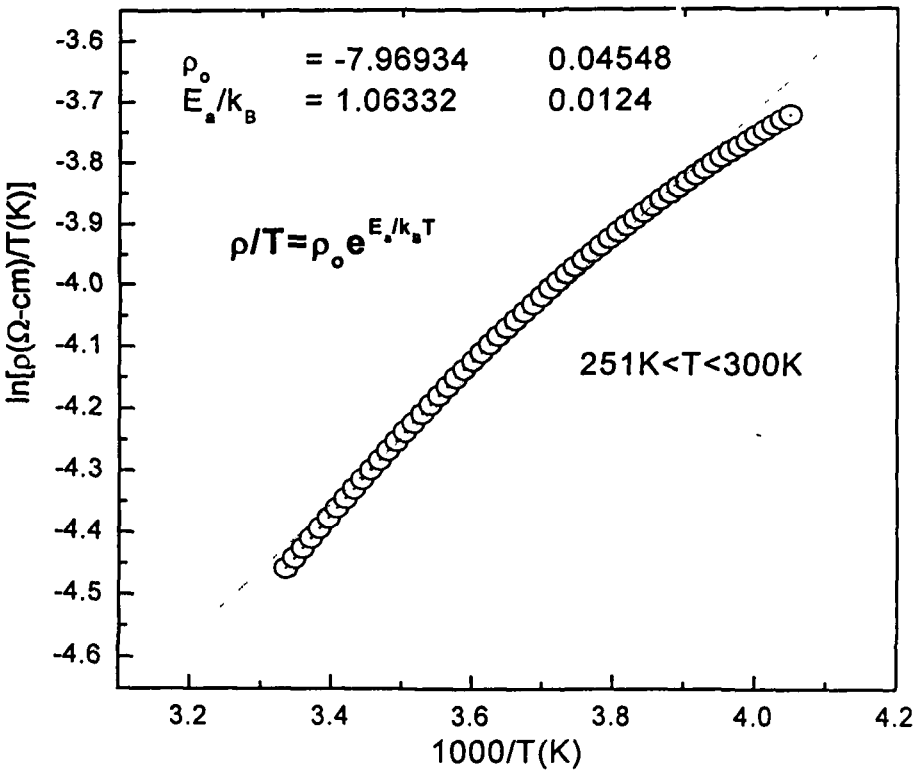

Fig. 3.5 (a) High Temperature dependence of resistivity for $La_{0.75}Sr_{0.25}MnO_3$.

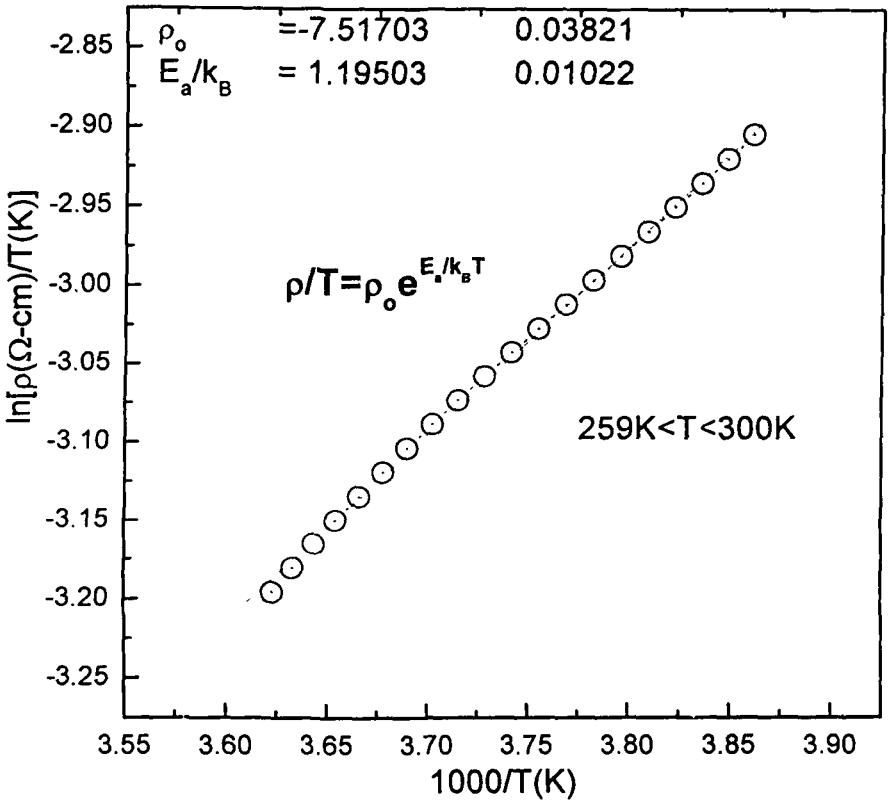

Fig. 3.5 (b) High Temperature dependence of resistivity for $La_{0.67}Sr_{0.33}MnO_3$.

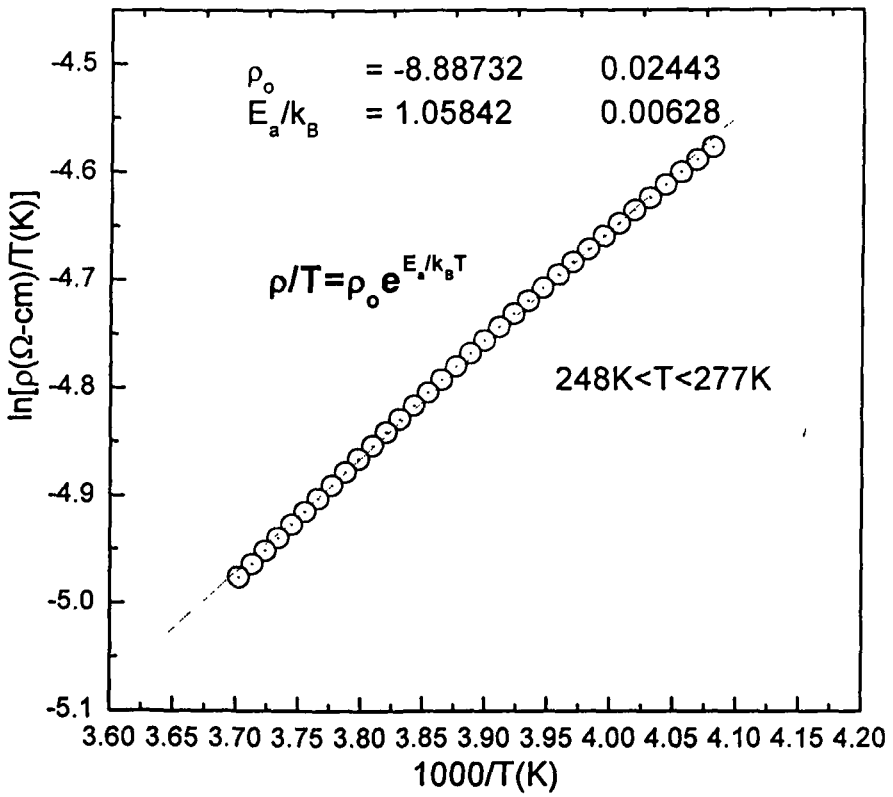

Fig. 3.5 (c) High Temperature dependence of resistivity for $La_{0.75}Sr_{0.25}MnO_3$.

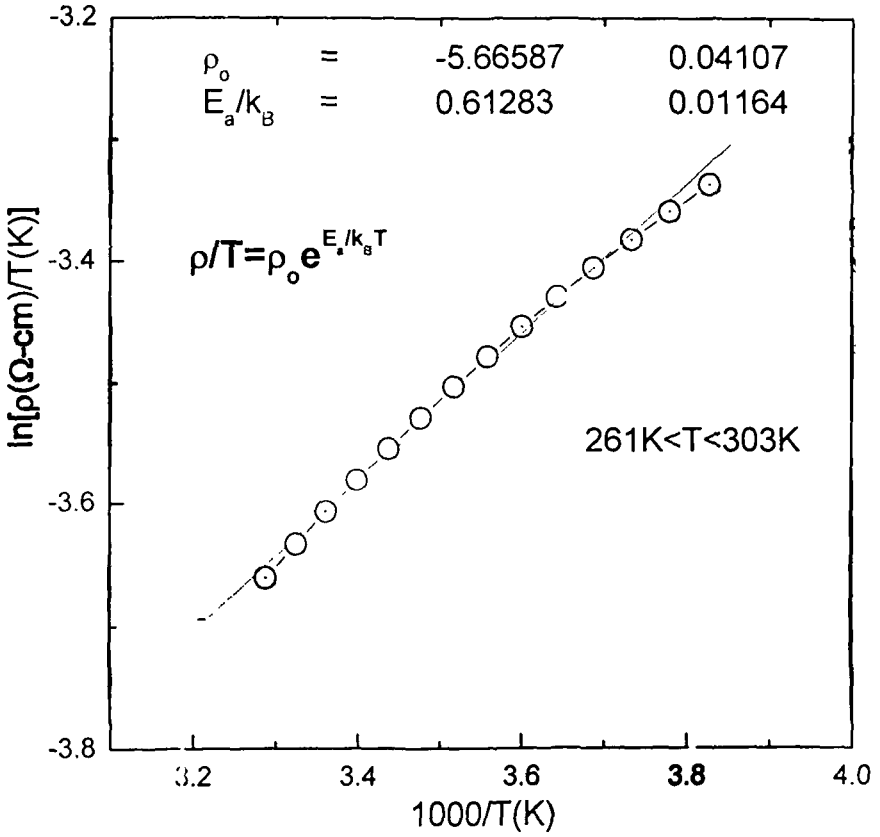

Fig. 3.5 (d) High Temperature dependence of resistivity for $La_{0.67}Sr_{0.33}MnO_3$.

The activation energies calculated using plots shown in Figs. 3.5 (a), 3.5 (b), 3.5 (c), 3.5 (d) are found to be respectively $0.916875\times10^{-4}\pm0.0124$ eV, $1.0307\times10^{-4}\pm0.01022$ eV, $0.912\times10^{-4}\pm0.00628$ eV and $0.5285\times10^{-4}\pm0.01164$ eV.

3.7 MAGNETIC PROPERTIES:

Fig. 3.6 (a) and 3.6(b) show the isothermal dc magnetization hysteresis at 300 K (Room temperature) for $La_{0.75}Sr_{0.25}MnO_3$ and $La_{0.67}Sr_{0.33}MnO_3$ samples prepared by Solid-State reaction-route as well as Sol-Gel method respectively upto the maximum available field of 10000 (Oe.). In Fig. 3.6 (a) maximum magnetizations are 1.84 and 1.70 (emu/cm^3) for 25% Sr doped samples. Whereas, in Fig. 3.6 (b), the maximum magnetizations are

maximum available field of 10000 (Oe.). In Fig. 3.6 (a) maximum magnetizations are 1.84 and 1.70 (emu/cm^3) for 25% Sr doped samples. Whereas, in Fig. 3.6 (b), the maximum magnetizations are 2.54 and 1.75 (emu/cm^3) for 33% Sr doped samples. It is clear from the figures that the magnetizations don't saturate till 10000 (Oe.) fields. The magnetization results are also in agreement with XRD and resistivity results. The hysteresis loop magnetization measurements are intrinsically bulk measurements.

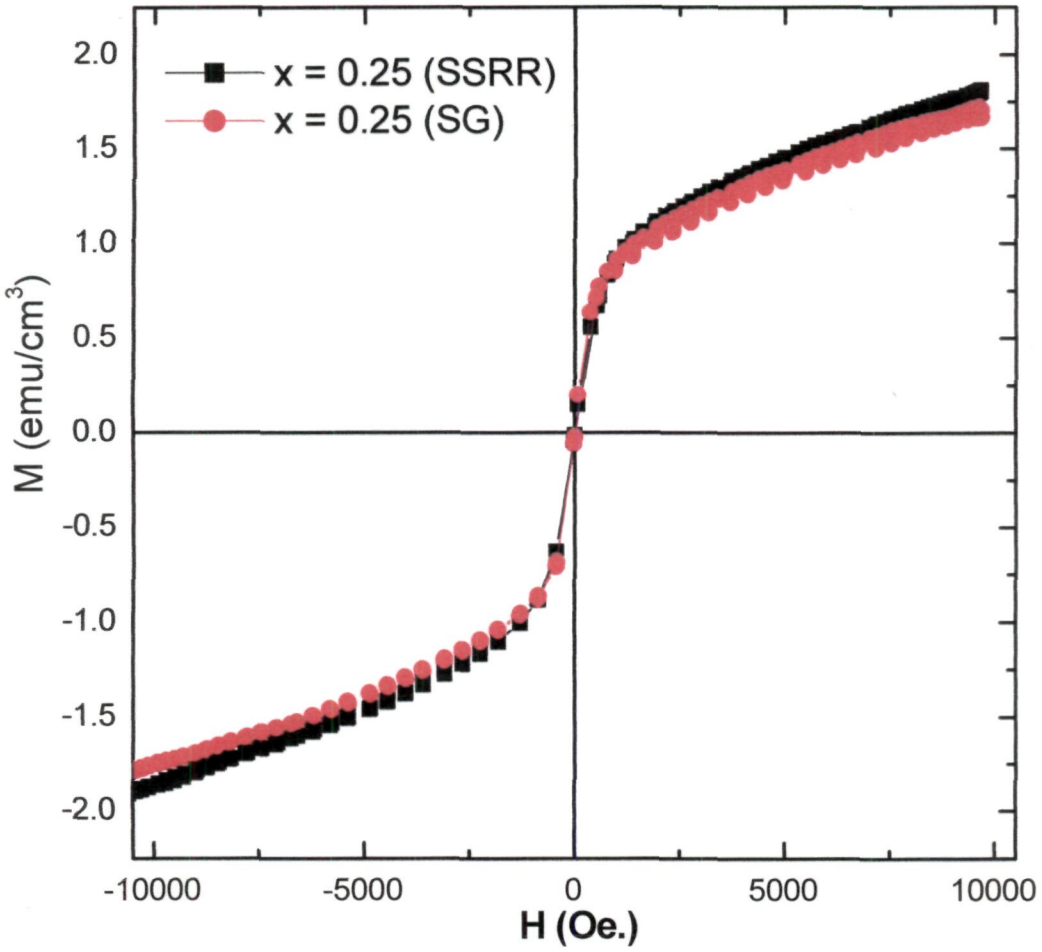

Fig 3.6 (b) M-H Curve for $La_{0.75}Sr_{0.25}MnO_3$ samples

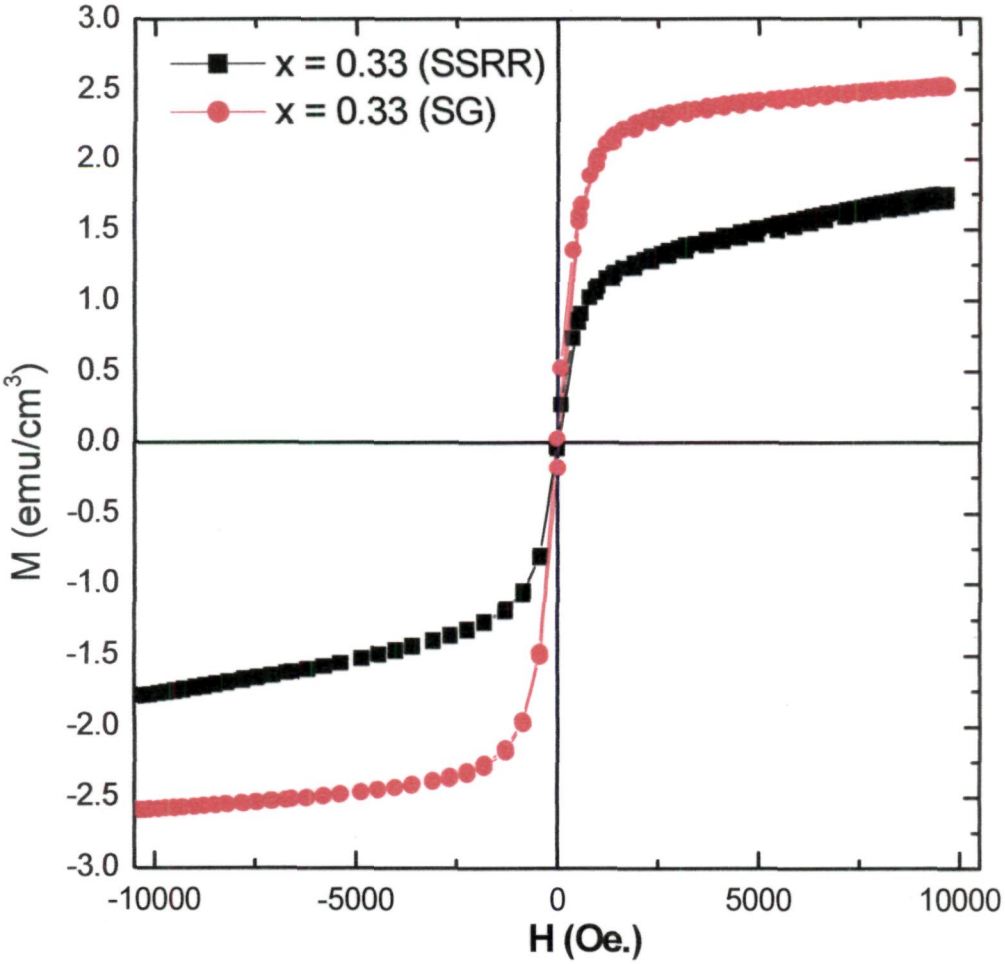

Fig 3.6 (a) M-H Curve for $La_{0.67}Sr_{0.33}MnO_3$ *samples.*

REFERENCES

1. J. Phy. : Condenced Matter **19** (2007) 196218
2. Coey, J.M.D., Vivet M. And von Molnar S, Advance Physics, **48** (1999) 167
3. Goodenough J.B., Zhou J.S., Rivadullah F and Winker E., J. Solid-State Chemistry **175** (2003) 116
4. Mott N.F. and Devis E.A. 1979 Electronic Processes in Non-Crystalline Materials (Oxford: Oxford University Press).
5. Okunev V.D., Samoilenko Z.A., Pafomov N.N., D'yachenko T.A., Plehov A.L., Szymczak R., Baran M., Szymczak H. And Lewandowski S.J. Phys. Lett. A **346** (2005) 232
6. A. Banerjee, S. Pal, B.K. Chaudhuri, J. Chem. Phys. **115** (2001) 1550
7. G. Venkataiah, P. Venugopal Reddy, J. Magn. Magn. Mater. **343** (2005) 285
8. G.J. Snyder, R. Hiskers, S. DeCarolis, M.R. Beasley, T.H. Geballe, Phys. Rev. **B53** (1996) 14434
9. J.M. De Teresa, M.R. Ibarra, J. Blasco, J. Gorcia, C. Marquina, P.A. Algarabel, Z. Arnold, K. Kamanev, C. Ritter, R. von Helmolt, Phys. Rev. **B54** (1996) 1187
10. M. Domonguez, S.M. Bhagat, S.E. Lofland, J.S. Ramachandran, C.G. Xiong, H.L Ju, R.L Greene, T. Venkatesan, Eur. Phys. Lett. **32** (1995) 349
11. A. Urushibara, Y. Moritomo, T. Arima, A. Asamitsu, G. Kido, Y. Tokura, Phys. Rev. **B51** (1995) 14103
12. G. Venkataiah, P. Venugopal Reddy, Solid-State Communication, **114** (2005) 136.
13. T. Holstein; Ann. Phys. (N.Y.), **8** (1959) 343
14. D. Emin; Electronic Structure Properties of Amorphous Semiconductors, edited by P.G. Le Comber and N.F. Mott (Academic New York, 1973)
15. D.C. Worledge, G. Jeffrey Snyder, M.R. Beasly, T.H. Geballe, R. Hiskers and S. DiCaroluis; J. Appl. Phys., **80**, 5158, (1996)

CHAPTER-4

CONCLUSIONS

4.1 INTRODUCTION:

In this dissertation we studied the structural, electrical and magnetic properties of Sr doped $LaMnO_3$. We summarize our results in this chapter.

4.2 STRUCTURAL PROPERTIES:

The pure LaMnO3 is found to be orthorhombic. On doping with Sr at the La site the lattice parameters changed considerably but the doped compounds remain in the orthorhombic symmetry. The unit cell volume sometimes decreases and sometimes increases with the increasing Sr concentration and reaches a value of 229.916Å^3 for the end member $La_{0.50}Sr_{0.50}MnO_3$ of the series prepared by Solid-State reaction-route and a value of 239.858Å^3 for the end member $La_{0.60}Sr_{0.40}MnO_3$ of the series prepared by Sol-Gel method, while in case of pure $LaMnO_3$ the value is 238.982 Å^3.

4.3 TRANSPORT PROPERTIES (BULK SAMPLES):

We measured the temperature dependence of resistivity of $La_{1-x}Sr_xMnO_3$ (x = 0.25, 0.33, 0.40, 0.50 for Solid-State reaction-route and x = 0.25, 0.33, 0.40 for Sol-Gel method) down to liquid nitrogen temperature. On processing the samples at higher temperatures, we could observe only a single transition. Although, the double transition in temperature dependence of resistivity was also observed by the earlier workers which is associated with the impurity or secondary phase. The single transition indicates to a better quality of our samples compared to those synthesized by the earlier workers.

4.4 FUTURE PLAN:

The electrons in the solid interact with one another and also with lattice vibrations. During the last few years, a lot of attention has been given to the electronic structure of 3d transition metal oxides. The interesting point in all

these 3d transition metal oxides is that on varying the electronic configuration of the 3d shell, their electrical and magnetic properties vary. Our integrated plan of research work for the Ph.D. programme shall proceed on the following lines.

1. Preparation of the following bulk samples by Solid-State reaction-route and by Sol-Gel method both.

   (i) $La_{1-x}Zr_xMnO_3$

   (ii) $Pr_{1-x}Ca_xMnO_3$

   where $x = 0.0, 0.1, 0.2, 0.3, 0.4, 0.5, 0.6, 0.7, 0.8, 0.9$ and 1.0.

2. Characterization of bulk samples by following techniques.

   (i) XRD- To study the structure of these materials.

   (ii) Electrical Resistivity- It will be measured by four-probe technique in the temperature range from 4.2 K to 300 K with the applied magnetic field. It is to examine the Metal-Insulator transitions temperature (T_{MI}) and transport phenomenon.

   (iii) Mössbauer study- To understand the site occupancies of La and Pr ions and the magnetic structure of the sample.

   (iv) XAS- It is also interesting to study the electronic atomic structure using synchrotron radiation source.

   (v) Magnetization study as a function of temperature and magnetic field to understand the magnetic properties of these materials.

   (vi) Preparation of thin film by Pulsed Laser Deposition (PLD) technique and characterization of unirradiated thin film by above mentioned techniques.

(vii) Irradiation of thin films (two samples each series) by Gold, Oxygen and Nickel ion beam.

3. Characterization of irradiated thin film by above mentioned techniques.

Our aim in this work is to irradiate the thin films and study the effect of the structural strain induced effect on the transport and magnetic properties of these materials and correlates them with the disorder induced localization in these materials, which could provide new insight in the field of magnetic materials.

Our XRD, temperature dependence of resistivity and M-H curves have sufficient information to suggest that Sr doped $LaMnO_3$ can be formed in single phase under properly controlled conditions.